Stony Brook University

Synchrotron White Beam X-ray Topography Study of EFG Sapphire Ribbons

A Thesis Presented

by

Zheyu Li

to

The Graduate School

in Partial Fulfillment of the

Requirements

for the Degree of

Master of Science

in

Materials Science and Engineering

Stony Brook University

May, 2014

Stony Brook University

The Graduate School

Zheyu Li

We, the thesis committee for the above candidate for the

Master of Science degree, hereby recommend

acceptance of this thesis.

Michael Dudley – Thesis Advisor
Professor, Department of Materials Science and Engineering

Balaji Raghothamachar – Second Reader
Research Professor, Department of Materials Science and Engineering

T. A. Venkatesh– Third Reader
Associate Professor, Department of Materials Science and Engineering

This thesis is accepted by the Graduate School

Charles Taber
Dean of the Graduate School

Abstract of the Thesis

Synchrotron White Beam X-ray Topography Study of EFG Sapphire Ribbons

by

Zheyu Li

Master of Science

in

Materials Science and Engineering

Stony Brook University

2014

Sapphire (α-Al_2O_3) is well-known as an important technological material primarily for the application as substrates for GaN based LEDs (Light emitting diodes). Additionally, sapphire is also characterized by properties such as high transparency, excellent scratch- resistance, chemical stability, high mechanical strength, good thermal conductivity and electric insulation. These make it attractive for wide use as optical windows, bearings, armor protections etc. The structure of sapphire is rhombohedral (a = b = c = 5.13 Å, $\alpha = \beta = \gamma = 55.1°$). But it can also be considered as pseudo-hexagonal (a = b = 4.759213Å, c = 12.9915867Å, $\alpha = \beta = 90°$, $\gamma = 120°$). The crystal structure is a slightly distorted hexagonal closed-packing of large oxygen ions (O^{2-} anions) with small aluminum ions (Al^{3+} cations) occupying two thirds of octahedral interstices.

The sapphire samples in this study were grown by the Edge-defined film-fed growth (EFG). Compared to other growth techniques such as Czochralski method, Kyropoulos method, heat exchanger method, the EFG method offers the advantage of obtaining near final shape of single crystal sapphire wafers. However, the growth conditions must be optimized to obtain low defect density ribbons. Therefore, to understand defect nucleation and propagation in these crystals, Synchrotron White Beam X-ray Topography has been employed in conjunction with optical microscopy and chemical etching in this study. Of particular interest in EFG sapphire is the nucleation of polycrystallinity that lowers yield.

Transmission X-ray topography reveals the overall defect distribution around the region of polycrystallinity and the range of tilts and strains. Section X-ray topography is used to trace the evolution of strain and/or dislocations leading to onset of polycrystallinity. X-ray reticulography is used to quantitatively map the variation in strains and tilts around the region of polycrystallinity. All defects found in sapphire will be specifically discussed regarding their formation, effects and behaviors with the characterization techniques described.

Table of Contents

List of Figures

List of Tables

List of Abbreviations

LAGB	low angle grain boundary
HAGB	high angle grain boundary
HCP	hexagonal close packed
FCC	Face Center Cubic
BCC	Body Center Cubic
EFG	Edge-defined film-fed growth
SWBXT	Synchrotron White Beam X-ray Topography
BPD	basal plane dislocation

Acknowledgments

First I would like to give my deep and sincere gratitude to Professor Michael Dudley, my advisor, for providing me this great opportunity to study in the field of defect characterization and stress analysis. His wide knowledge and helpful guidance have been of great value for me. No doubt his understanding, encouragement and personal guidance have always been providing an excellent basis for my research.

I would like to thank Dr. Balaji Raghothamachar, valuable suggestion and discussion during the entire research project. And he is the one I worked with a lot. His guide to doing experiments leads me walking into the field of Synchrotron White Beam X-ray Topography.

I would like to thank Professor T. A. Venkatesh for being in my committee member and his help and suggestion during my research project.

I would also like to thank my colleagues: Ms. Huanhuan Wang, Mr. Fangzhen Wu, Mr. Jianqiu Guo, Mr. Goue Ouloide Yannick, Ms. YuYang, Mr. Zihao Ding and Ms. Ruifen Chen for their help.

Finally, I would like to thank my parents. They give me this great opportunity to studying in United States. They encourage me and give life suggestions to me during my entire life. Without them, I can’t go this far for now.

Chapter 1 Introduction

1.1 Structure of sapphire and properties

Sapphire (α-Al_2O_3) is popularly used in the industry of LED as substrates of GaN epilayer growth. It is highly transparent, excellent scratch- resistant, chemical stability, high mechanical strength, good thermal conductivity and electric insulation. Sapphire is also widely used as optical windows, bearings, armor protections etc. Table 1.1 lists the properties and applications of sapphire.

Table 1.1 Sapphire: properties and applications [1].

Properties	Parameters	Applications
Hardness	Mohs: 9	Knives, scratchproof window
Melting point	2303K	Aerospace, Countermeasures lamps, Illumination windows
Density	3.98 g/cm^3	
Optical transmission range	0.17-5.5 μm	FLIR (Forward Looking Infrared) windows
Water absorption	None	Observation windows, sensor
Young Modulus	345GPa	
Shear Modulus	145GPa	
g -radiation stability	No change in transmission above 2.5 mm after exposure to 107 Rads. No visible coloration after exposure to 108 Rads/hr for 60 minutes at - 195°C	NMR (Nuclear Magnetic Resonance) tubes
Proton radiation stability	No change in transmission below 0.3 μm after exposure to 1012 proton/cm^2 total dose	Optical components: lenses, prisms and other laser
Chemical resistance	Sapphire is highly inert and resistant to attack in most process environments including hydrofluoric acid and the fluorine plasma applications	Endoscope lenses, erosion resistance windows
Solubility -In water -In HNO3, H2SO4, HCl, HF -In alcalis -In melts of metals Mg, Al, Cr, Co, Ni, Na, K, Bi, Zn, Cs	Insoluble; Insoluble to 300°C; Insoluble to 800°C; Insoluble to 800-1000°C;	erosion resistance windows, sensor components, etc.

The structure of sapphire is rhombohedral. However, it is considered as pseudo-hexagonal as well. If consider the O^{2-} anions as balls, the crystal lattice takes the form of their closest hexagonal packing (Figure 1.1 a). The Al^{3+} cations are located in the octahedral sites enclosed by 6 O^{2-} anions. Only two-thirds of the sites are filled [2]. The coordination number of Al^{3+} is 6 and for O^{2-} is 4. Both Al and O have different but repeating layers of spatial arrangements along the third axis, i.e., the structure is completely replicated in six O^{2-} layers and six intermediate Al^{3+} layers (Figure 1.2 a). The central pair of Al^{3+} ions (AB), three equivalent neighboring pairs (AC), three equivalent remote pairs (AD), and six equivalent most remote pairs (AE) are shown in this figure. In the direction of the C-axis, the three distances Al–O are equal to 1.97 Å and the other three distances are 1.87 Å. The Al–Al and O–O spacing are 2.65 Å and 2.52–2.87 Å, respectively [3].

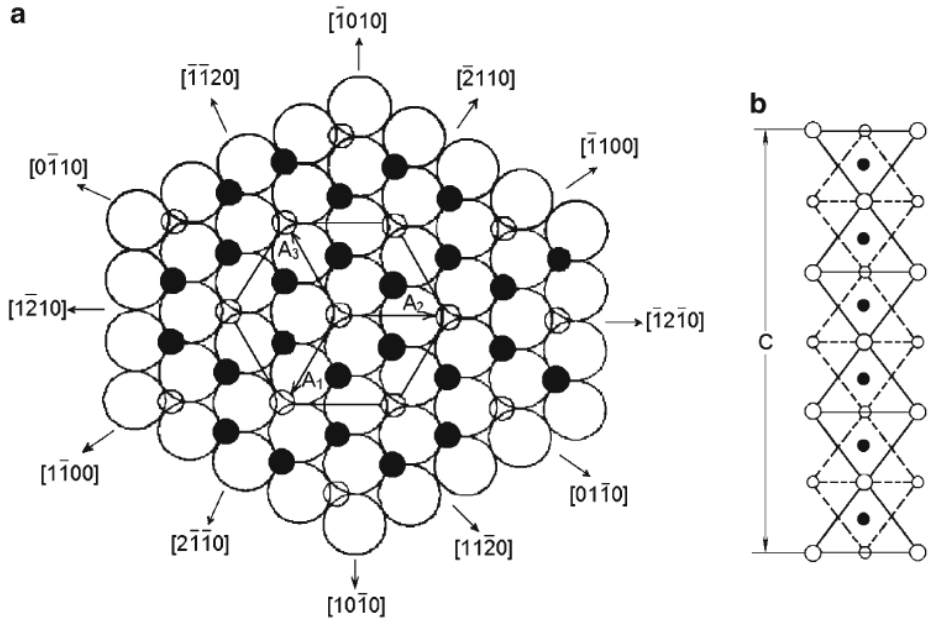

Figure 1.1 (a) Schematic of the arrangement of Al^{3+} (black circles) and octahedral hollows (small light circles) between two layers of O^{2-} (large light circles) in the basal plane (the upper O^{2-} layer is not shown). A_1, A2, and A3 are <11-20> translational vectors of the hexagonal sapphire cell for the basal plane. (b) Schematic of the packing of O^{2-} ions (light circles) and Al^{3+} in the direction of the axis C_3 [2].

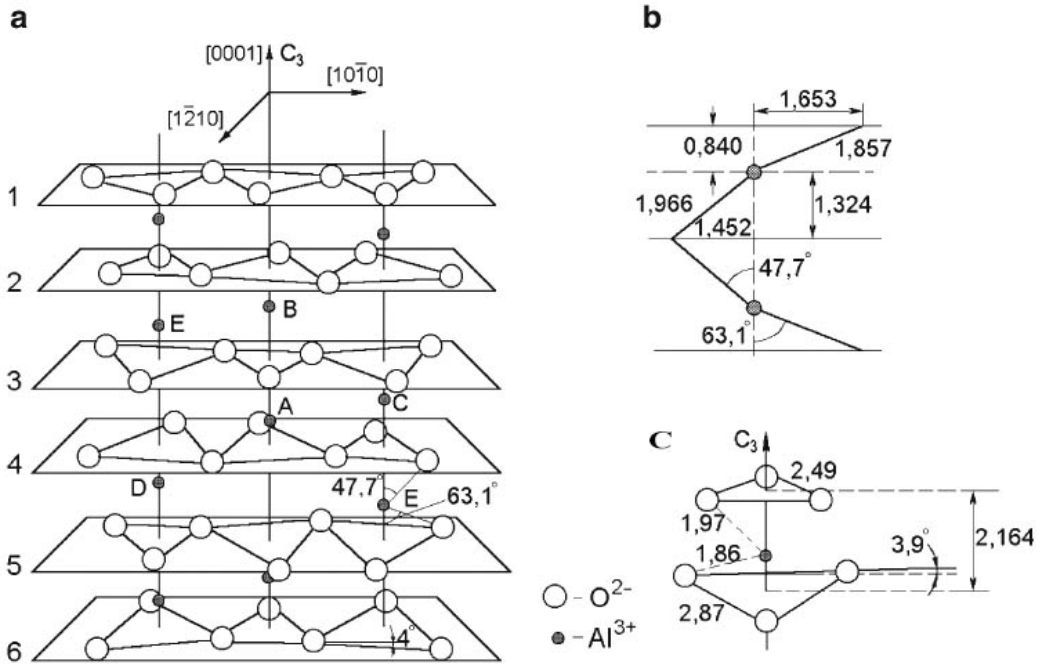

Figure 1.2 (a) Schematic of the arrangement of Al^{3+} ions and O^{2-} layers (black circles); (b) the distance between Al^{3+} and O^{2-} ions; (c) the position of O^{2-} ions surrounding Al^{3+} ion. The planes of the triangle are perpendicular to the C-axis [3]

To better understand, Figure 1.3 (a) presents a schematic of the rhombohedral structure in the pseudo-hexagonal structure. And (b) is Sapphire crystal structure constructed using Crystal-Maker. These figures illustrate the relationship between rhombohedral structure with pseudo-hexagonal structure.

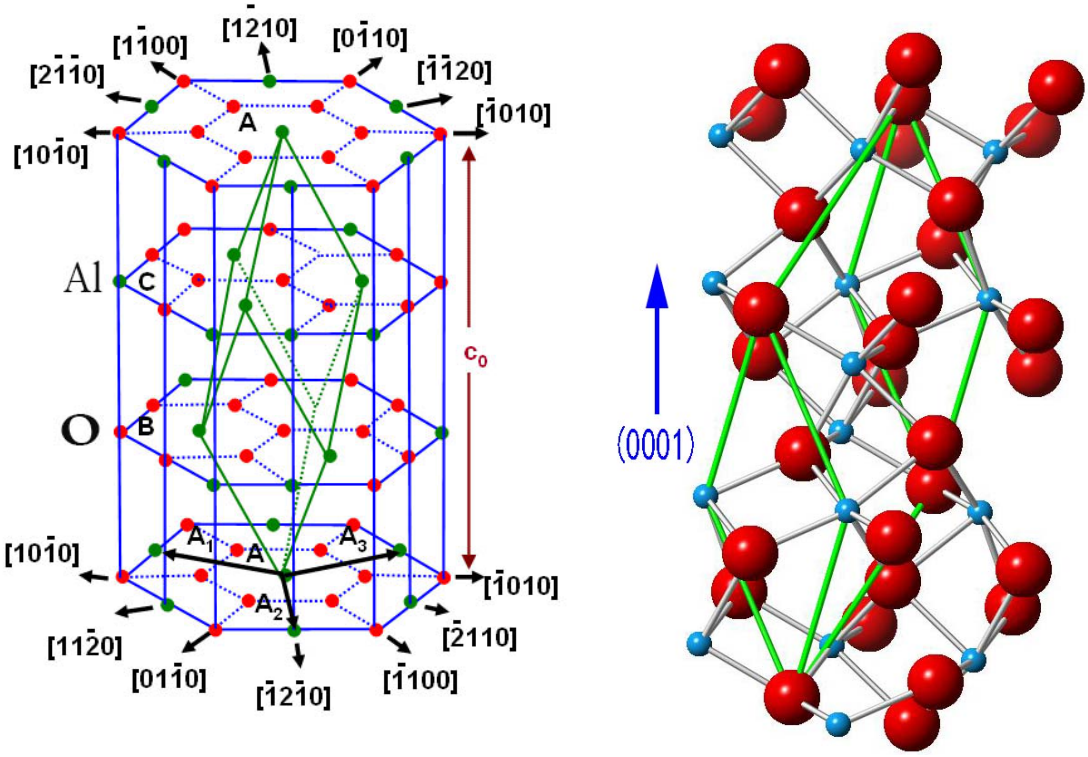

a) b)

Figure 1.3 Comparison between pseudo-hexagonal with rhombohedral in sapphire (a) The green atom is Al, and the red one is O as labeled. The green rhombohedron inside the hexagonal structure is the unit cell of sapphire when it considered as rhombohedral structure [4]. (b) Sapphire crystal structure constructed using Crystal-Maker, the red atom is O, and blue one is Al. The green lines present the rhombohedral unit cell.

1.2 Defects in sapphire

1.2.1 Point defects

Basically, there are three major types of point defects in sapphire, which can be divided into five different situations.

a) Frenkel disorder: equal number of vacancies on Al sublattice and formation of Al interstitial atoms.
b) Frenkel disorder: equal number of vacancies on O sublattice and formation of O interstitial atoms.
c) Schottky disorder: equal number of vacancies on Al and O sublattice.
d) Schottky disorder: equal number of Al and O interstitials.
e) Antistructure disorder: substitutional disorder where Al atoms occupy O sites and O atoms occupy Al sites [5].

One perfect crystal array and five schematics of point defect for simplest MX compound are presented in Figure 1.4, just for easily understanding.

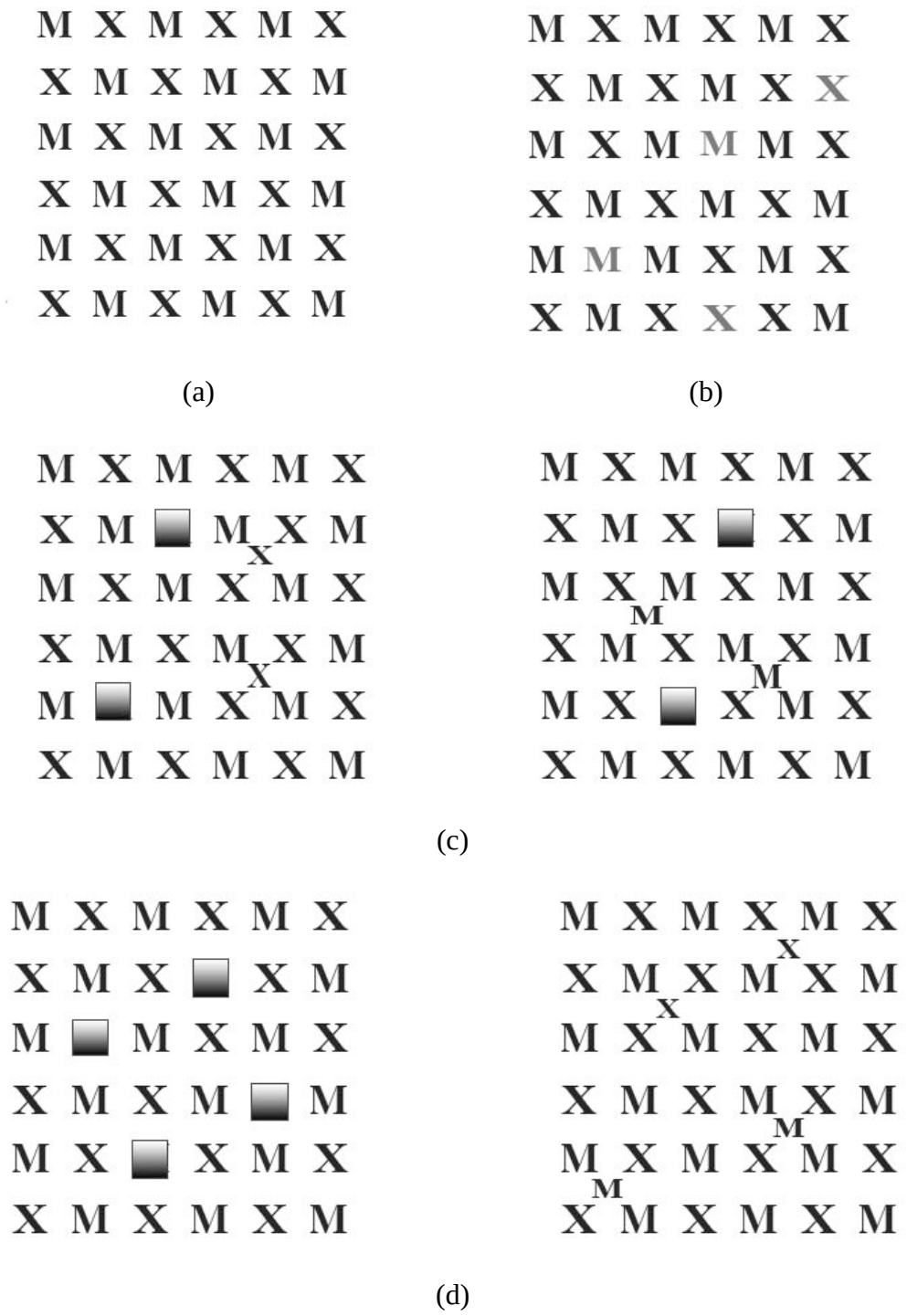

Figure 1.4 (a) Perfect MX crystal array, (b) Antistructure disorder, (c) Two types of Frenkel disorders, and (d) Two types of Schottky disorders.

1.2.2 Dislocations

The most common way to define a dislocation is the Burgers vector using a Burgers Circuit, which is a closed loop, connected by atom to atom, enclosing the dislocation in the loop. At the same time, apply the same atom-to-atom sequence to a perfect crystal area. It turns out the second circuit cannot be closed. And the additional step to close the loop is named Burgers Vector, presented as **b.** It includes information on both the direction and length of dislocation. Figure 1.5 presents two Burgers Circuit to explain how the Burgers Vector is defined.

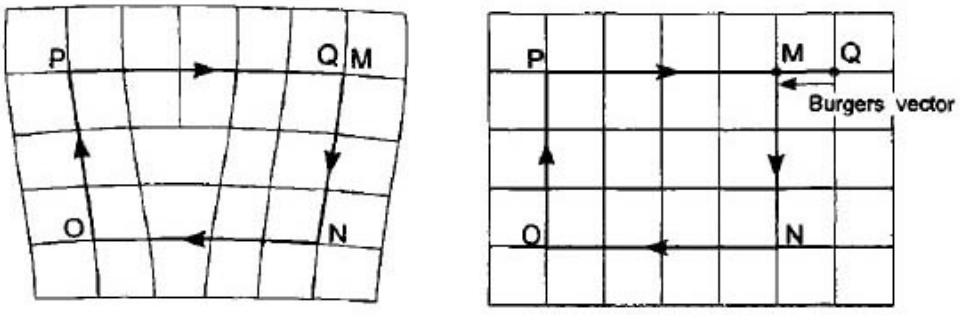

Figure 1.5 Circuits in both imperfect and perfect crystal to define Burgers Vector [8].

And for perfect dislocation, the shortest repeat lattice distance is its Burgers Vector. In sapphire, perfect dislocations with **b** = 1/3<11-20>, 1/3<10-11> and <10-10> have been found and studied.

The dislocations with **b** = 1/3<11-20>, called basal dislocations, since they usually occurs on basal plane (0001), to constitute basal slip. And the basal slip (0001) 1/3<11-20> is primary slip system, which dominates at high temperature below the melting point. The Burgers vector **b** = 1/3 <11-20> have the lowest energy in sapphire crystal among all perfect dislocations. They are most easily formed by high temperature plastic deformation. So the basal slip requires lowest critical resolved shear stress when the temperature is above 700 °C [6].

The dislocations with **b** = <10-10> are called prism plane dislocations. With high energy, the prism plane dislocations are unexpected. Dissociating the dislocation into two dislocations, by the following reaction, can decrease the energy:

$$\langle 10\text{-}10\rangle \longrightarrow 1/3\langle 2\text{-}1\text{-}10\rangle + 1/3\langle 11\text{-}20\rangle \qquad \text{Equation 1}$$

The reason dislocation with **b** = <10-10> is still stable may be the Burgers Vector corresponds to a closed-packed direction of the oxygen sublattice, to lower the Peierls barrier, coupled with the dissociation into three collinear partials which obviously have a high mobility [6].

$$\langle 10\text{-}10\rangle \longrightarrow 1/3\langle 10\text{-}10\rangle + 1/3\langle 10\text{-}10\rangle + 1/3\langle 10\text{-}10\rangle \qquad \text{Equation 2}$$

In addition, the dislocations with **b** = 1/3<10-11> are named rhombohedral dislocations. Their energy is a little bigger than basal dislocations. Their Burgers Vectors are the smallest out of basal plane. Although these dislocations form and multiply on pyramidal planes, they do not exactly lie in any specific pyramidal plane. They can be found in low angle grown-in subgrain

boundaries, but more frequently, they form prominent components in the dislocation substructures due to irradiation damage [6].

1.2.3 Planar defect

Planar defects include grain boundaries, stacking faults and twin boundaries.

Grain boundaries

Grain boundaries bound the grains in a crystal. Each grain is a single crystal, and misoriented with respect to the others. Grain boundaries can be broadly classified into two types in general, which are low angle grain boundaries (LAGBs) and high angle grain boundaries (HAGBs). Grain boundaries with less than 10° misorientations are generally considered as LAGBs, while those with more than 10° are HAGBs.

Stacking faults

Stacking faults, as the name suggests, are disturbances of normal atoms arrangement by change in the regular stacking sequence. They are observed in different structures, but most commonly found in closed-pack structures, such as {0001} planes in hexagonal close packed (HCP) structure, and {111} planes in Face Center Cubic (FCC) structure. And the stacking sequence of HCP is ABABAB, which means after first two atom layers, the third atom layer lies on the directly above A atom layer. So, if the third atom layer lies on the C position, then the stacking fault on HCP structure is formed as the sequence of ABABCABAB.

On the other hand, the third atom layer for FCC structure does not lie over the A atom layer, rather choosing the C position. Therefore, the regular stacking sequence of FCC structure is ABCABCABC. If a part of C atom layer is missing, the stacking sequence changes to ABCAB_ABC, which is intrinsic fault. The second possibility is inserting additional atom layer into regular sequence, named extrinsic fault, for example, ABCABCABC changes to ABCABACABC by adding A atom layer. The schematic diagram showed in Figure 1.6.

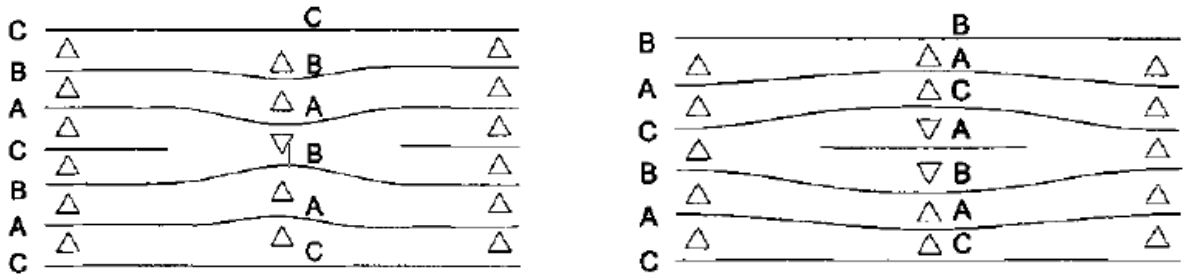

(a) (b)

Figure 1.6 Two types of staking fault in FCC structure, (a) Intrinsic fault; (b) Extrinsic fault [7].

Twin boundaries

Twin boundaries separate regions of a crystal having a definite orientation relationship. The symmetry operations could be 180º rotation about an axis, or reflection over a plane, which are twin axis and twin plane as defined [8]. Based on how twins originate, they can be classified into three types, which are annealing twins, growth twins and deformation twins.

Annealing twins are usually formed after cold-working when metals are annealed to recrystallize. They have a rotation axis, around which the two parts of crystal are symmetric. Taking FCC structure for example. The atom sequence of FCC structure is ABCABC… During annealing period, recrystallization occurs. The continuous growth sequence should be ABCABC-ABCABC. If the sequence changes to ABCABCBACBA, the new growth crystals are still FCC structure. But the new sequence has a mirror symmetry with respect to the original crystal and therefore is the twin of the parent crystal. If the sequence reverses back to the original crystal at the next stage, we get ABCABC-BACB-ABCABC stacking. Thus the -BACB- layer forms a twin band [8].

The growth twins are caused by an accidental departure from equilibrium during growth, and, favored in the nucleation stage, especially under conditions of supersaturation. In general, during crystal growth, atoms locate in positions, which can lower their energy most to keep themselves stable. However, atoms also take positions where it is close to the minimum energy level. These atoms do not continue the old stacking pattern of crystal, and if they are formed immediately, a twin may persist [9].

The so-called deformation twins are usually caused by shear stress in plastic deformation [9]. The applied shear stress on the crystal creates a new orientation by gliding. Two twins crystals are produced in mirror symmetry. Figure 1.7 illustrates the mechanism of formation of deformation twins [8].

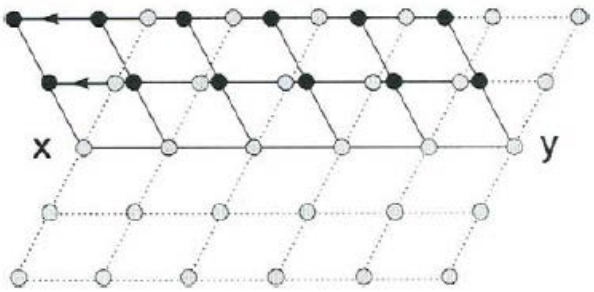

Figure 1.7 Open circles are the original position of crystal; black circles are the position after twinning. Under applied shear stress, the crystal yielded and new orientation created by gliding. X-Y is the symmetry plane of twins [8].

Volume Defects

Volume defects occur in a much bigger scale, such as voids, precipitates and bubbles. And it also includes cracks and secondary phases. All these defects can happen in certain conditions and play important role on the properties of crystal [8].

1.3 Growth method

Crystal growth is a process of crystallization to obtain single crystals. There are several different methods, depending upon initial growth condition, which could be molten, vapor phase,

solutions, gels, etc. The crystallization process generally also involves changes in pressure, heated, and sometimes use crystal seed.

1.3.1 Kyropoulos method

Kyropoulos (KY) method was initially developed by Kyropoulos in 1926, then, improved by Musatov in 1970's. Kyropoulos method is an effective and mature way used to grow large size sapphire single crystals. Crystal seed is used in this process. When the seed contacts with the melt, crystallization begins. And the whole process can be divided into several steps, which are seeding, shouldering, equal diameter growth, annealing and cooling. Kyropoulos method is very unique, because under low temperature gradient in hot zone, the crystallization has sharply convex front. And the shape of crystal is irregular and almost fills whole crucible. The crystallization steps and the schematic of furnace are showed below [10].

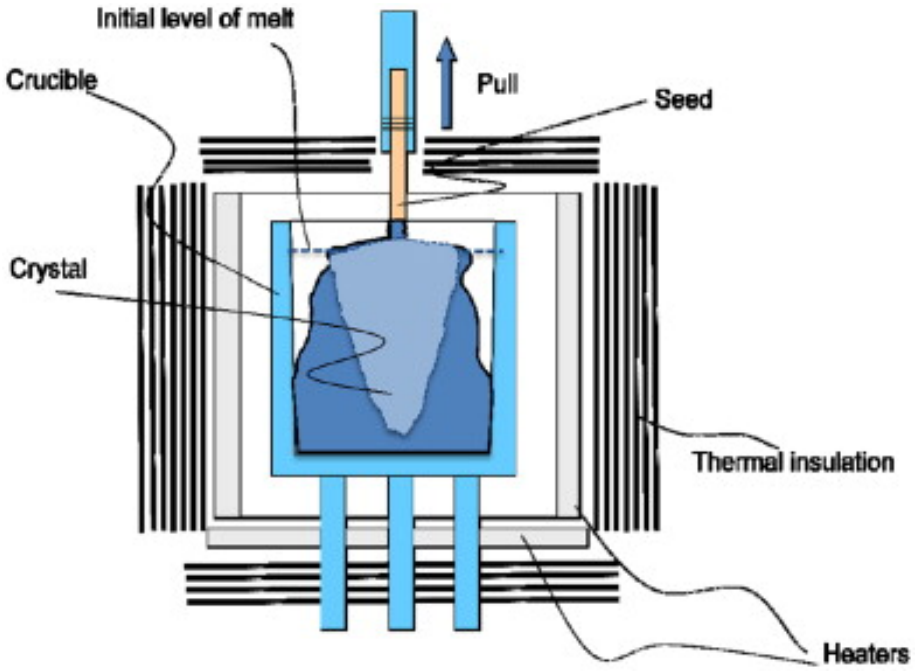

Figure 1.8 Furnace of Kyropoulos growth method. A short pull up is applied at the beginning of the crystallization, when the seed touching the melt [10].

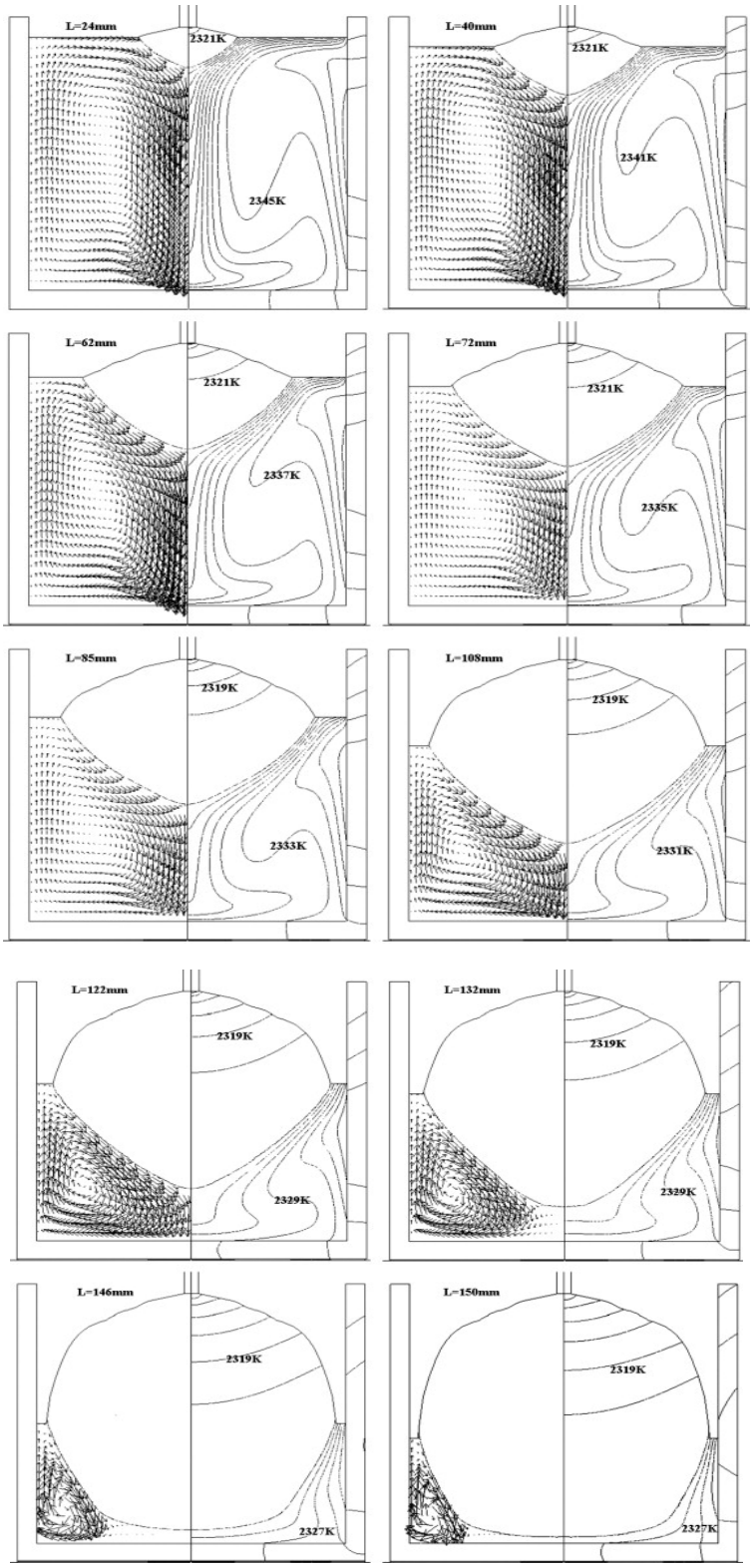

Figure 1.9 Isotherms (right-hand side) and velocity vectors (left-hand side) at different growth stages (temperature fields in the crystal region are T_{max}=2323 K, Δ T=−2 K and in the melt region they are T_{min}=2323 K, Δ T=2 K) [11].

1.3.2 Heat exchange method (HEM)

The heat exchange method (HEM) was firstly designed by Fred Schmid and D.Viechnicki at the Army Materials Research Lab in1967 [12]. The so-call heat exchange is because the system has heat exchanger which is filled with helium gas. By adjusting the flow speed of helium gas, the crystallization process can be controlled. The seed is place on the bottom of crucible, and the crystallization process also starts from the bottom and proceeds all the way to the top. After the seed starts to melt, the flow speed of helium increases, from the bottom to the hot zone, to help crystallization onto the seed. When the crystallization is completed, the boule is subject to annealing, and the temperature and gas flow are both reduced at the same time. Since the temperature gradient is really low, the quality of crystal is comparatively good with low density of dislocation and bubbles.

To control the cost, the furnace is made up of molybdenum crucibles, graphite heating elements and graphite porous insulation. After finishing annealing, the crucible is broken to take out the bulk crystal. However, since the graphite is used in the system, there is oxygen deficiency in the crystal [13].

(a) (b)

Figure 1.10 HEM sapphire boules, 34 cm diameter, 65 kg (a) after growth still in the crucible, and (b) after removal from the crucible [13].

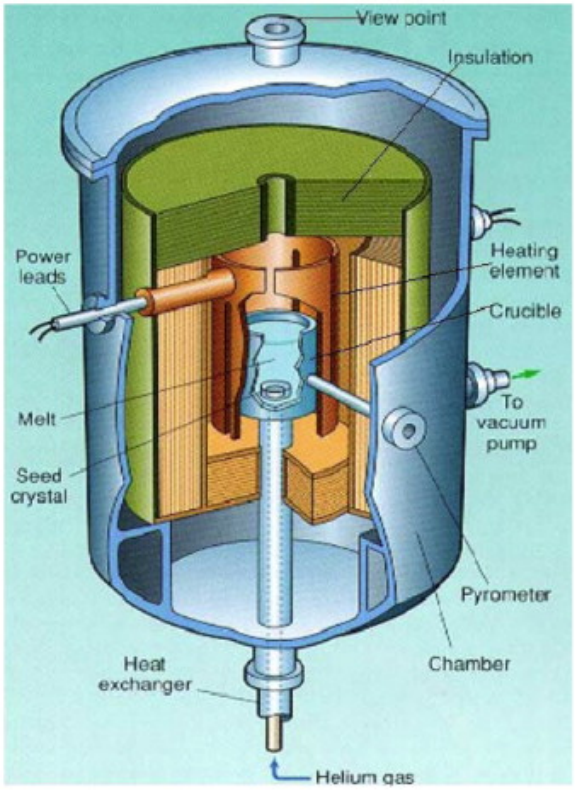

Figure 1.11 Schematic of an HEM furnace [13]. Helium gas enters from the bottom to hot zone.

1.3.3 Czochralski method (Cz)

Cz growth method was originally invented by Jan Czochralski in 1910, then modified by Teal, Little and Buehler from Bell Labs. After many years developing, Cz method becomes one of the mainly used industrial crystal growth methods. However, since it is difficult to grow sapphire crystal along C-axis, and the size of crystal also becomes bigger and bigger, the Cz method is not suitable for modern industrial requirements.

The Cz growth method requires pulling and rotation during the whole process. The seed is placed at the end of the pulling rod, with certain orientation, at the interface of the melt at beginning. The furnace has a feedback system, which the weight of the crystal can be measured. Then the modulation of heater power according to the crystal weight controls the expansion profile and the final size of sapphire. The temperature gradient of Cz method is high, because the convex crystal interface is below the melt level during the all process [13]. A schematic diagram of Cz furnace is shown in Figure 1.12.

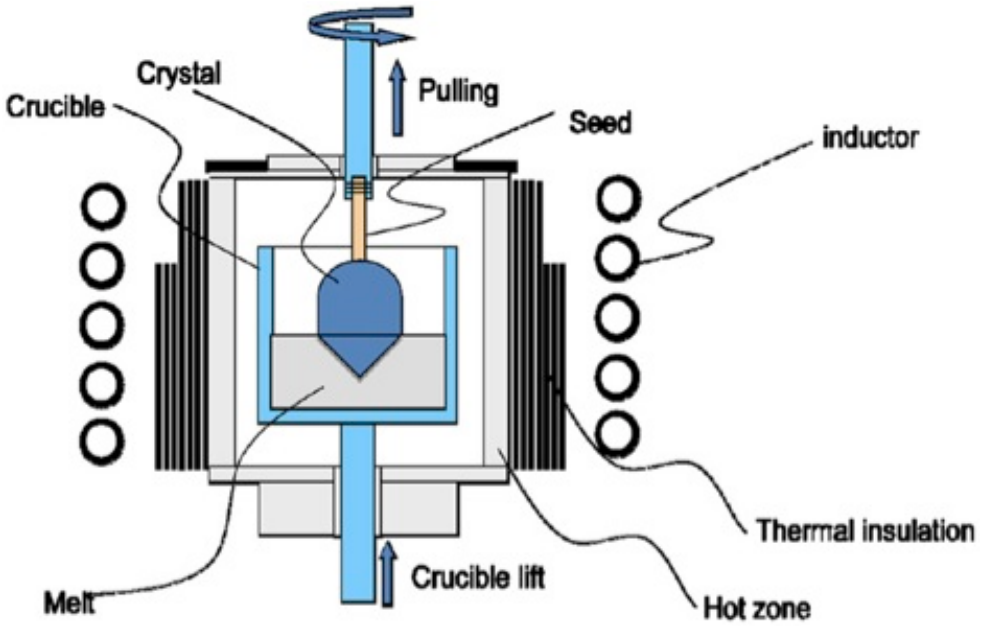

Figure 1.12 Schematic diagram of Cz growth process. The rod is constantly pulled and rotated. The convex crystal interface is always lower than the melt level.

1.3.4 Edge-defined film-fed growth (EFG)

Edge-defined film-fed growth (EFG) is a unique technique which can grow designed shaped crystals, such as ribbon, tubal and nemaline crystals. Harold Labelle and Stepanov originally developed it in 1960's [14]. The main features of EFG grow method are (1) crystallization mold is used during the process; (2) the melt is driven by capillary force all the way to the top of mold to crystallize; (3) the height (size) of the crystal is determined by the melt viscosity and the driven force; (4) the growth speed of EFG is fast and multiple pieces of crystal can be produced at the same time. The Figure 10 depicts the schematic diagram of EFG growth process.

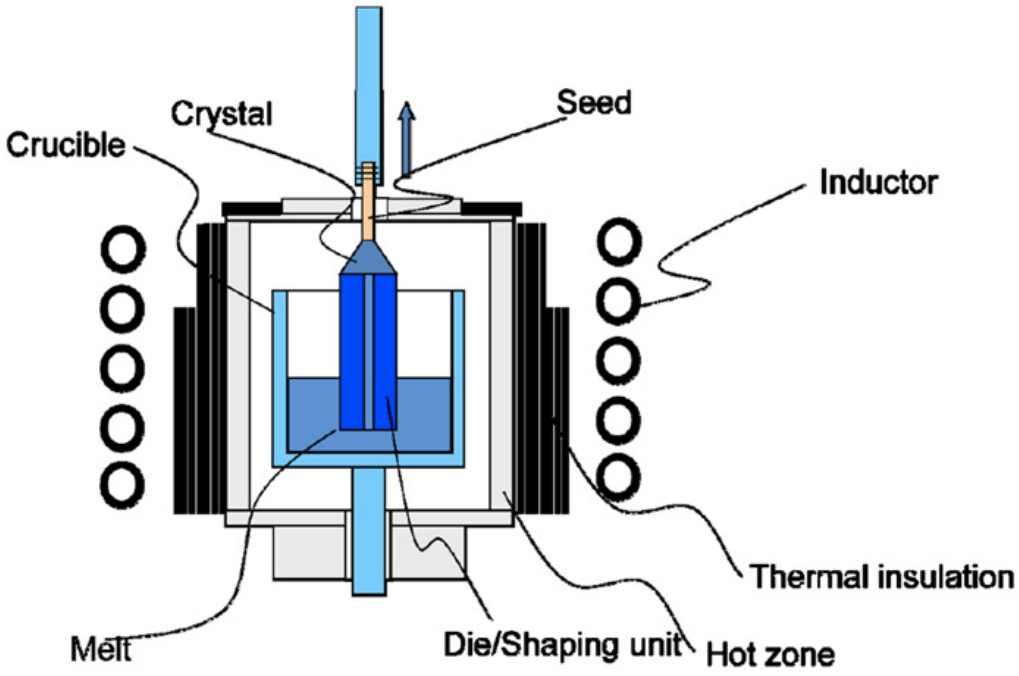

Figure 1.13 Depict the schematic diagram of EFG growth method

The reason the technique is named Edge- defined is that the edge of die limits the edge of growing crystal, which means either the shape of die or the outer edge of top die surface determines the shape of the growing crystal [13]. In another words, if the top surface of the model is bigger than the cross-section of the seed, the growing crystal will gradually enlarge to the edge of model, as the seed is pulled up. Since the melt is driven up through the die, which is thin film of melt, the temperature inside the die must be controlled carefully. Otherwise, the crystallization in the die will stop the growth process. The disadvantages of EFG growth method are higher dislocation density, bubbles close to surface when growing ribbons, the residue stress is pretty high and grain boundaries often appear in crystal [13].

Chapter 2 Experimental methodology

In the experiments, the techniques used to observe defects and characterization of structure basically are Synchrotron White Beam X-ray Topography (SWBXT), Chemical Etching and Optical Microscopy. Synchrotron White Beam X-ray Topography includes X-ray Transmission Topography, X-ray Grazing topography, X-ray Section topography and Reticulograph. In this chapter, each technique will be introduced, especially Synchrotron White Beam X-ray Topography, which was carried out at the National Synchrotron Light Source at Brookhaven National Laboratory.

2.1. Synchrotron White Beam X-ray Topography

2.1.1 Fundamental of Synchrotron White Beam X-ray Topography

With the booming development in semiconductor industries, the quality control and structural analysis is highly in demand. As a non-destructive technique, Synchrotron White Beam X-ray Topography is a powerful and important tool to help improve the quality of crystals by observing various defects directly. It is just a general term of a series of X-ray diffraction imaging techniques, which is based on Bragg's Law, defined as follows:

$$\lambda = 2d\ Sin\theta \qquad \text{Equation 3}$$

Where the λ is X-ray wavelength, d is lattice plane spacing, and θ is the angle between incident beam and diffraction lattice plane, which also called Bragg angle. Crystal sample is placed on the stage in the desired position and a collimated X-ray beam is incident at the desired angle with respect to the sample to constitute a Bragg angle. Then, the corresponding diffraction beam projects to the high resolution film. On the film, two-dimensional spots are obtained, which include information of variation of diffracted intensity which is depend on the local diffracting power and overall diffraction conditions. Defects and deformed surrounding area affect the local diffraction power, in the way of presenting the variations in intensity on the deformed area and the closed perfect area. Due to the variations of intensity, the film has different contrast and various types of defects also can be identified. More details can be obtained by interpreting the variation of contrast, such as line direction and Burgers vector of dislocation. All analysis is based on well-known understanding of mechanisms of contrast formation [15].

It reveals that Synchrotron White Beam X-ray Topography is better than many other techniques with the advantages below.

(1) Non-destructive technique
As mentioned before, X –ray Topography is non-destructive technique to observe defects or characterization analyze. Comparing to SEM, TEM or chemical etching, Synchrotron White Beam X-ray Topography is superior in this case. Samples can go to commercial market or continue to next research process.

(2) Big size sample and whole crystal bulk can be applied to study
The sample diameter can be as big as 300 mm (Kawadoet al., 2002), and the weight can be several kilograms (Raghothamachar B, Chen H, and Dudley M, 1998, unpublished) [15].

(3) Multiple diffraction spots recorded simultaneously
Incident white beam causes multiple diffractions from different lattice planes, and corresponding diffraction beams project to film to form multiple diffraction spots. These diffraction spot giving lots of information save experiment time and improve the efficiency. It also makes possible comparison analysis from different spots for the same defect or diffraction feature.

(4) Several geometry modes can be applied
There are three basic geometry modes to obtain specific diffraction images. For example, to get transmission geometry, place film on the back of sample, incident beam go through the sample, and the diffraction beam project to film. And if film is placed on the same side as the incident beam, the diffraction beam is reflected to the film, which is back-reflection. By setting sample on designed position to constitute small incident angle, the near-surface information can be obtained, which is grazing. Certain geometry setting up is required to obtain different working models. The schematic diagrams of three geometry modes are presented below.

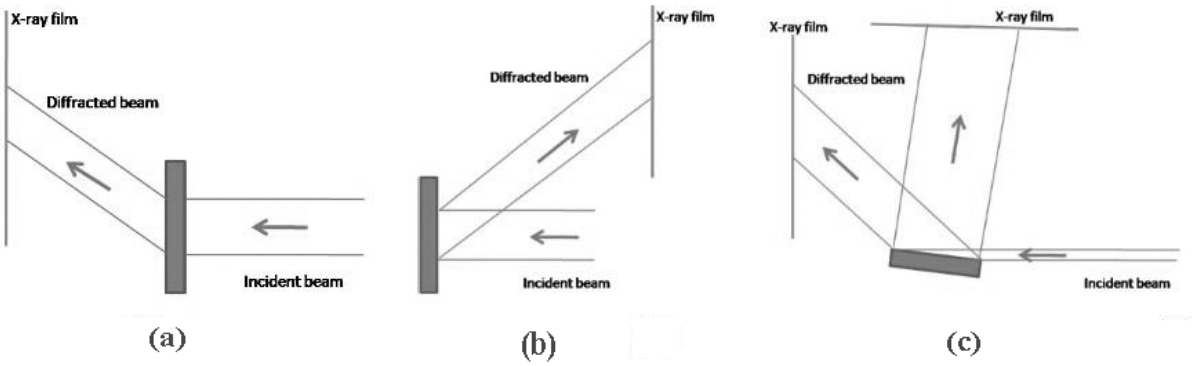

Figure 2.1 The schematic diagrams of three geometry modes: (a) transmission, incident beam goes through sample, then diffraction beam project to film from the back of sample; (b) back-reflection, film placed in front of sample, incident beam is reflected from the front surface of sample, projected on the film; (c) grazing. film placed over the sample; incident beam has sample angle respect to sample surface, which slightly penetrates into sample surface, then diffraction beam carried out to the film.

2.1.2 X-ray Transmission Topography

Transmission geometry is the most commonly used mode in Synchrotron White Beam X-ray Topography for relatively thin sample. As showing in Figure 2.1 (a), the basic principle of transmission geometry is incident beam go through the sample. The diffracted beam is projected to the film behind the sample, with a sample-film distance 50mm~250mm. The thickness of sample affects the topography recorded. Transmission geometry is not so effective for some

thick samples since the incident beam can be absorbed by the thick sample, which reduced diffracted intensity.

Scanning is often used in transmission geometry when certain reflection spot is needed for large samples. A lead plate with a slit is placed in front of the film to get the specific reflection spot. In order to select the required spot, Laue Pattern program is used. By setting the same geometry as the sample on the stage, the Laue Pattern program can simulate reflection spots obtained on the film.

2.1.3 X-ray Section Topography

A narrow slit is applied to restrict incident X-ray beam onto sample in X-ray Section Topography. Then narrow incident beam produces Bormann fan inside the sample, which is ABC as showed in Figure 2.2, the schematic of X-ray Section Topography. Then resultant diffracted beam projected to the film consists of Pendellösung fringes. Pendellösung fringes are parallel in case of a perfect crystal, or distorted in case of crystal with defects and/or strain. At high levels of strain, the fringes are no longer visible. Figure 2.3 presents experimental examples of Pendellösung fringes.

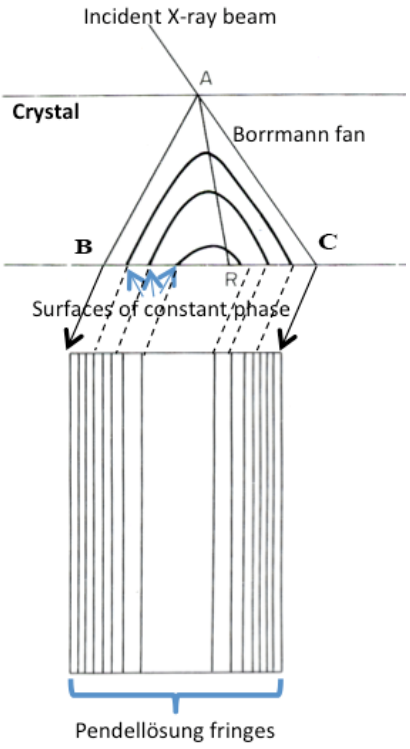

Figure 2.2 Schematic of X-ray Section Topography. ABC is Bormann fan; Pendellösung fringes are highly sensitive, which can only seen from high quality (almost perfect) crystal.

So the major advantages of applying X-ray Section Topography is small lattice strains can be observed, due to sensitivity of Pendellösung fringes. As a function of depth, it makes possible to locate defects [Lang, 1980]. In addition, stacking fault and tilt grain boundaries can be distinguished by using X-ray Section Topography [Capelle, et al., 1982].

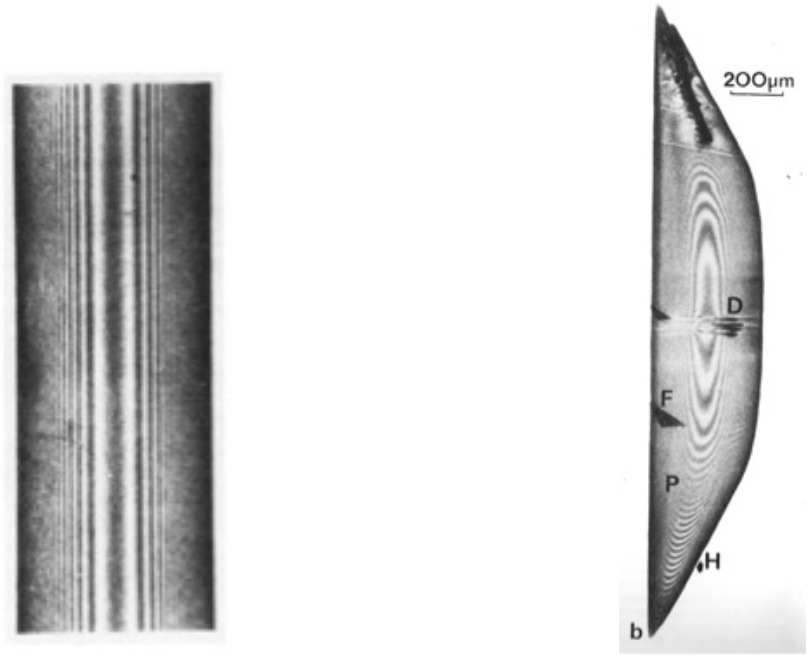

(a) (b)

Figure 2.3 (a).Pendellösung fringes in a section topography of a highly perfect silicon crystal (b). Perturbation of Pendellösung fringes in a section topography due to elastic strain from defects [16].

2.1.4 X-ray Reticulography

This technique is a similar to method of X-ray topography combining with an added element of grid made out of x-ray absorbing material, placed in the path of incident or diffracted beam. The grid essentially splits up the x-ray beam into numbers of micro-beams, the integrated image of all micro-beams forms a reticulograph. Each micro-beam can be traced in order to determine local plane normal using the principle of ray tracing. It can be applied to analyze the strain of sample, then, quantitatively analyzing residual stress. This technique is based on the hypothesis that there is a relationship between strain in crystal and local plane orientation. According to this relationship, full strain tensor can be determined as a function of position within the crystal. Then from the known strain tensor, the stress can be calculated by apply elastic constants of material [18]. As other usual X-ray Topography techniques, X-ray Reticulography also has several geometries depending on the experiment needs. Figure 2.4 is the transmission geometry of X-ray Reticulography.

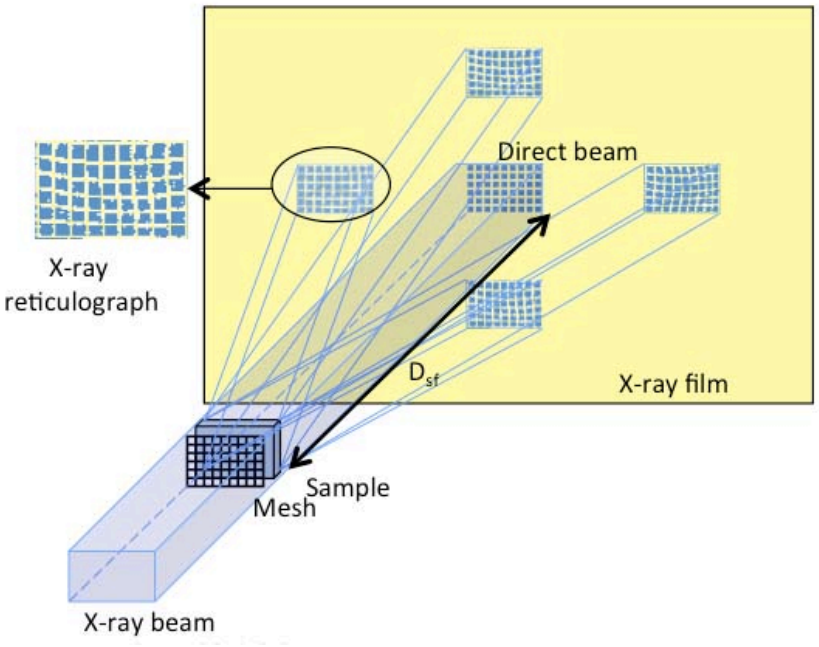

Figure 2.4 Schematic of transmission geometry of X-ray Reticulography. Incident beam go through mesh and sample, the beam is split into micro-beams, so as the reflections on the film.

Grazing geometry is used in this experiment, with a small grazing angle with respect to the incident beam. The grid is placed parallel to sample and just slightly above the sample. This grazing geometry can carry out the near surface deformation information. The schematic of grazing X-ray reticulography is showed in Figure 2.5.

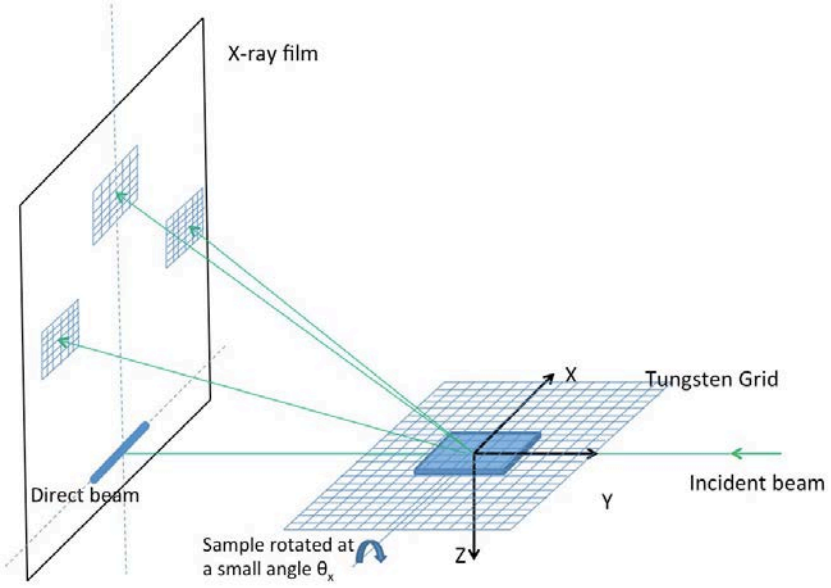

Figure 2.5 Schematic of grazing geometry of X-ray Reticulography. The grid parallels to the sample closely, sample rotated by a small angle, which is the incident angle of beam. Diffraction beam go through the grid, then split into micro-beams onto film.

2.2 Chemical Etching

Chemical etching, considered as one of the convenient and simplest techniques, is widely used in both research and industrial area.

For sapphire etching, the chemical commonly used is molten potassium hydroxide (KOH). Set temperature of oven at 410 ºC, add100% KOH solid particles into a Ni crucible, place the Ni crucible into oven. After 25 minutes, the solid KOH particles are molten, then carefully place the sapphire sample into the melt. The sample needs to be immersed completely for the entire etching period. In etching process, heating time for c-plane sapphire and m-plane sapphire are not the same. For c-plane sapphire, the heating time is 1 hour is required to form well-defined dislocation etch pits. However, the heating time for m-plane sapphire is much longer, because the dislocation properties on m-plane are different than for those on c-plane.

2.3 Optical Microscopy

Optical microscopy is also used in crystal defect analysis. By using optical microscopy, bubbles under the crystal surface could be studied. Figure 2.6 gives example of bubbles below the crystal surface. Under optical microscopy, surface morphology can be identified, such as steps left by dislocation movement to surface. Figure 2.7 presents steps on the surface as result of dislocation moving to surface. Moreover, optical microscopy combined with chemical etching to reveal dislocation pits, which will be discussed later.

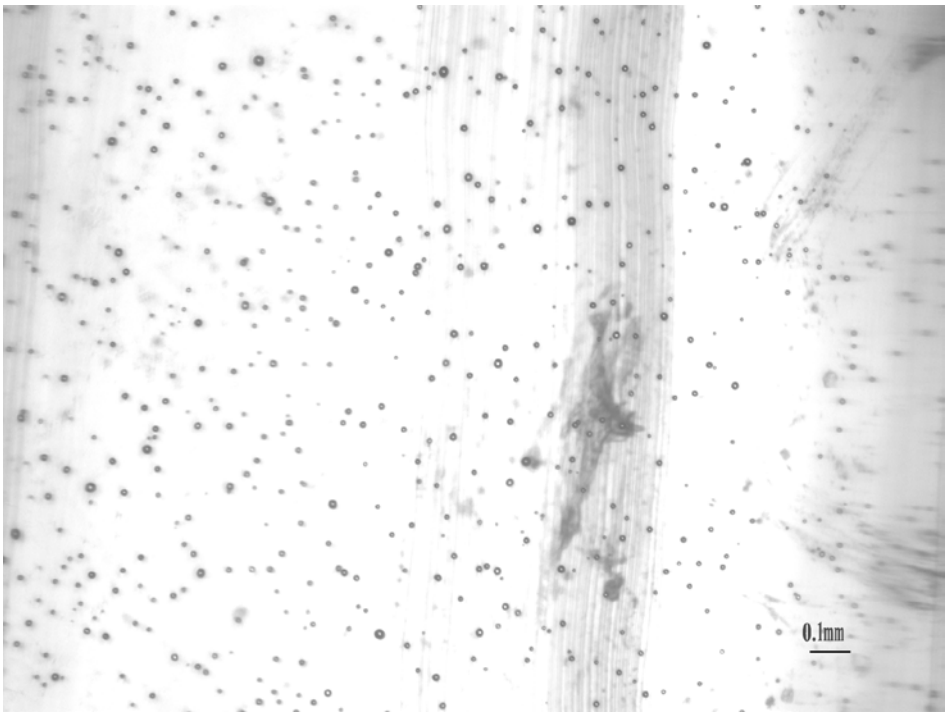

Figure 2.6 Bubbles (small circles) found in sapphire wafer by using Nikon Eclipse 600 W POL microscopy.

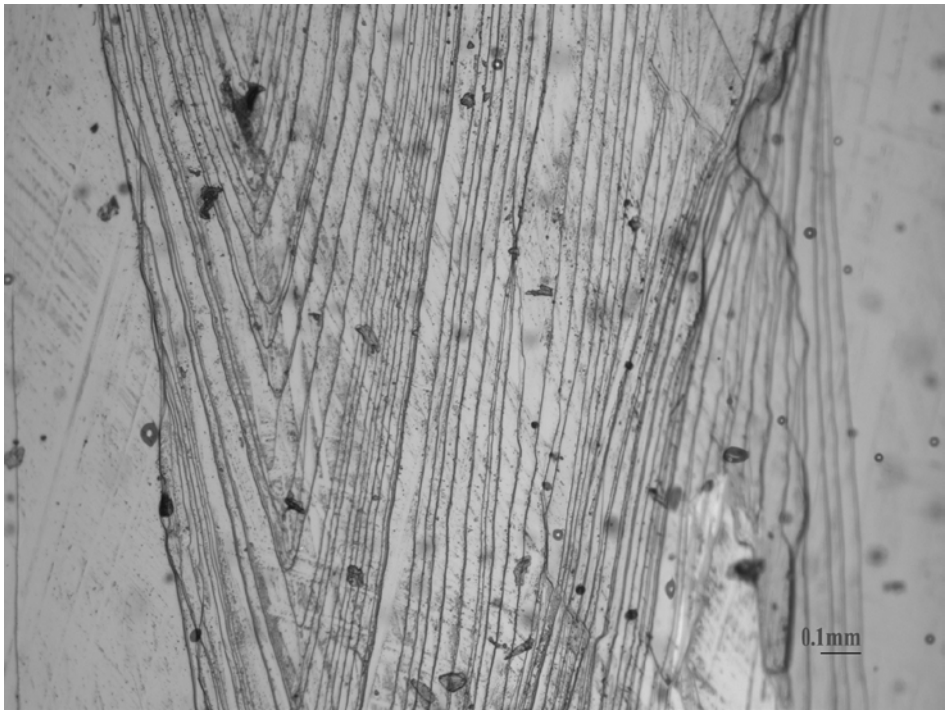

Figure 2.7 Steps on sapphire wafer surface observed by Nikon Eclipse 600 W POL microscopy. These lines are the steps left by dislocations completely moving to surface.

Chapter 3 Experiments and results

In this study, sapphire wafers are grown by edge-defined film-fed growth (EFG) method. And the shape of samples is ribbon. They are mainly studied by Synchrotron White beam X-ray topography at NSLS at BNL. The main purpose of this study is to understand the origins of the initialization of polycrystallinity by using X-ray topography in multiple modes in combination with other characterization techniques.

3.1 Seeds analysis

Since EFG method uses seed to grow crystal, and basal plane dislocations (BPDs) can replicate to the new crystal, the study starts from seed. Two seeds are studied by using Transmission X-ray Topography. As mentioned before, Laue Pattern program is used to simulate the diffraction pattern to select appropriate diffraction spots for recording X-ray topographs. We set up the transmission geometry parameters in Laue Pattern program with (1-100) surface, and side plane is (-1-120), the film sample distance is 190 mm, and the film size is 250 mm × 200 mm, then rotate sample about Y axis 10º to obtain the 11-20 reflection. The simulated diffraction pattern is shown in Figure 3.1.

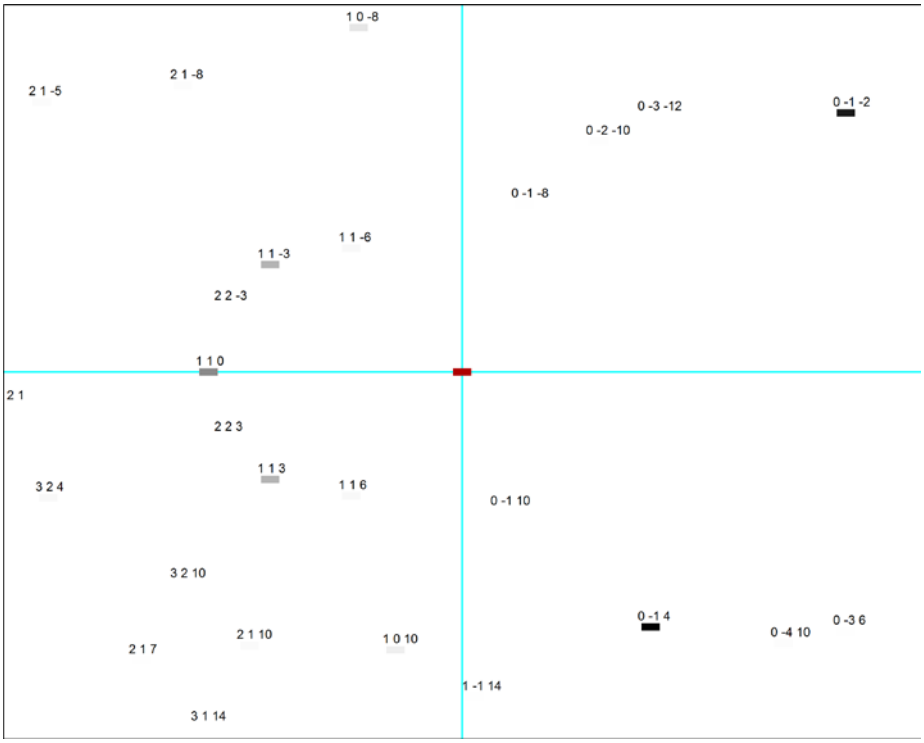

Figure 3.1 Simulated diffraction pattern from (1-100) sapphire seed sample and side plane (-1-120) after rotation by 10 about Y-axis.

In this case, we select reflection 110, which is 11-20 in four-index. At the same time, we use a fluorescent screen (same size as film) at the exact same position of film, to obtain the real reflection patterns. Carefully adjusting and reasonable guess is taken to get the same reflection

patterns as in the Laue Pattern program. The desired reflection 11-20 can be found on the fluorescent screen, at the similar position as the simulated reflection pattern. After obtaining the right reflection pattern, then the film can be loaded. Since the beam size is not big enough to cover the entire sample, the scanning mode is used to get whole reflection image. Reflection 11-20 is taken from 2 seed samples as shown in Figure 19. Fig 3.2 (a) is from an unused seed sample and Fig. 3.2 (b) is from a seed sample used for several growth runs.

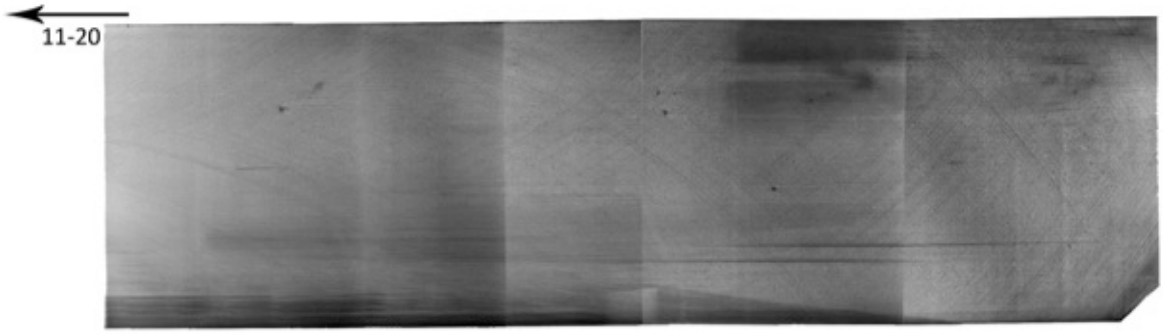

(a)

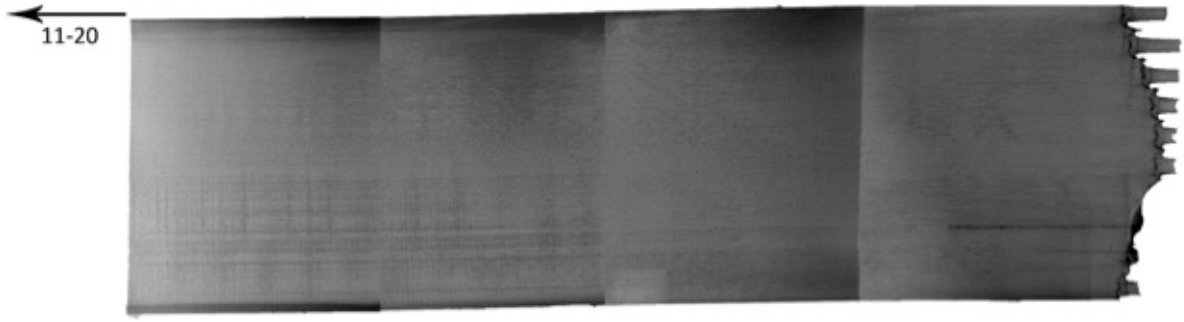

(b)

Figure 3.2 Transmission topography (g = 11-20), (a) is unused seed, (b) is used seed, with (1-100) surface, and (-1-120) side plane.

In these images, both seed samples are characterized by inhomogeneous distribution of basal dislocations. However, surface scratches obscure contrast from dislocations, especially in unused seed. So, some local magnified images are taken from those images for detail analysis in Figure 3.1.

From Figure 3.3 (a), we still can see some surface scratches marked by blue ellipses. From Figure 3.3 (b), we don't see obvious surface scratches as much as in (a). The reason the used seed having fewer scratches is probably because the scratches are healed due to annealing effect at elevated temperatures. From all these images, we could get one conclusion that the dislocation density is lowered as we go from the near growth end to the far end of growth.

Away from growth —→ close to growth

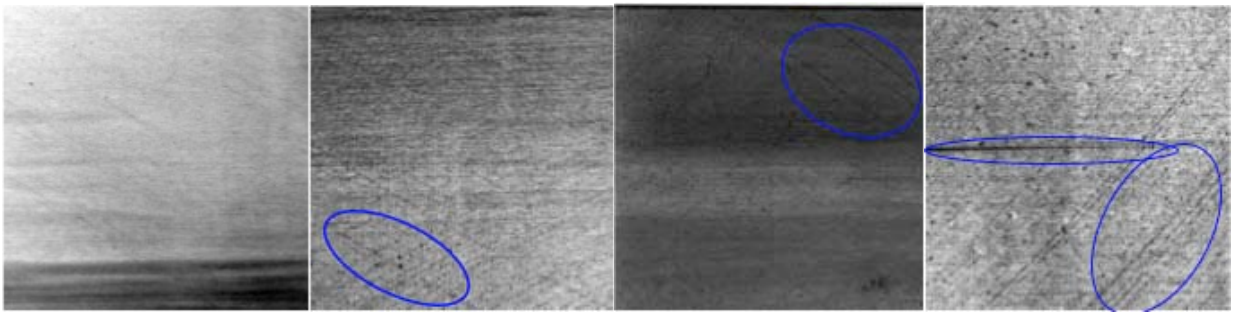

(a)

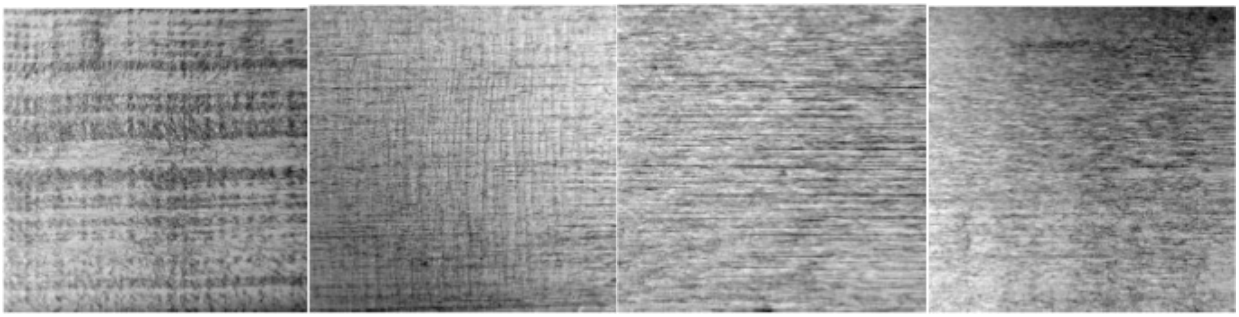

(b)

Figure 3.3 Detailed images taken from whole 11-20 transmission topographs, (a) four section parts from unused seed, (b) four section parts from used seed. Blue ellipses mark out the surface scratches on surface of unused sample, while the used sample cannot find obvious one.

We also observe, the third image of (a) from left side is significantly darker than the rest. Usually, the reason cause different contrast among different area is the change of diffraction intensity, which is generally explained in terms of two mechanisms: orientation contrast and extinction contrast. Basically orientation contrast arises from convergence (overlap) or divergence (separation) of diffracted rays. It happens since small angle grain boundary, twin and grain boundary, even misoriented lattice plane due to strains. The behavior of orientation contrast is either reinforcing or reducing the intensity. In this case, no twin or grain boundaries are observed, so the better explanation is high strains give rise to misorientation in lattice planes, which turns out changes in contrast of diffraction image [17].

Further study on unused seed is taken by transmission X-ray Topography in different reflections. Figure 3.4 gives comparison of 11-20 and 0006 reflections.

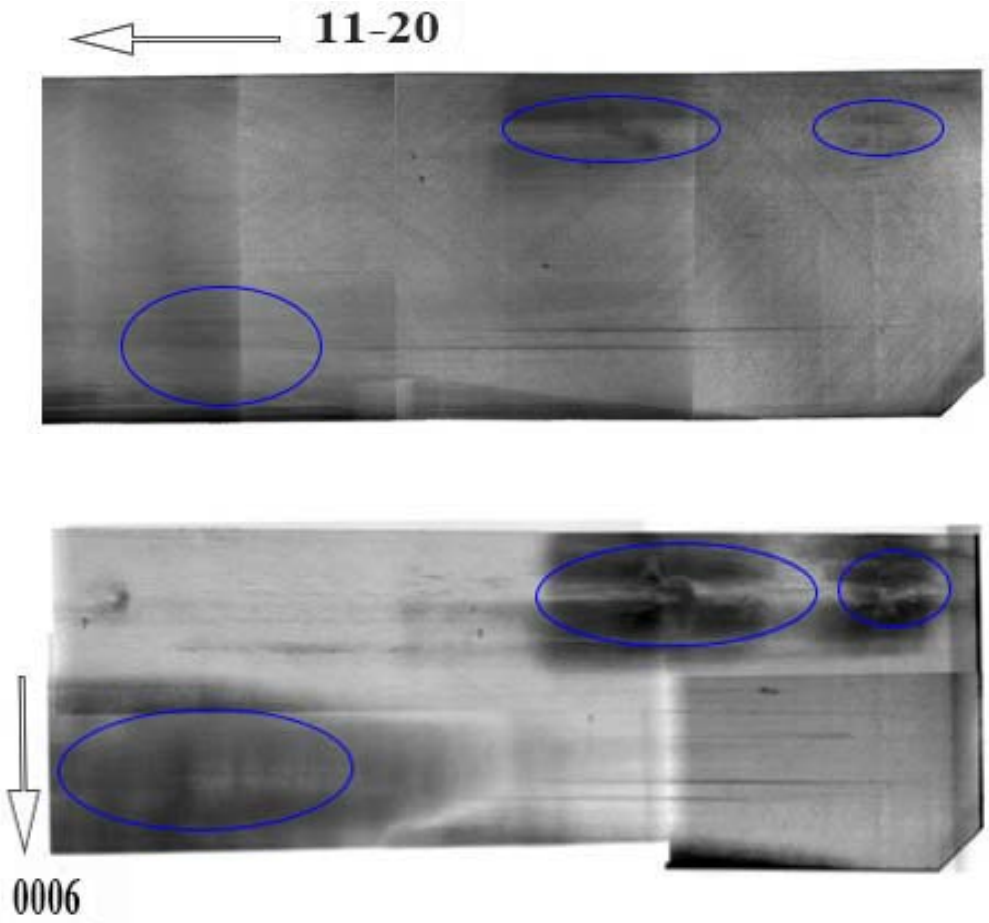

Figure 3.4 11-20 and 0006 reflections taken from unused seed on the same region. These blue ellipses are the region have high strains.

The dark areas are marked in both two reflection images, and turns out they are located on similar positions on different reflections, which means the high strain areas reinforce contrast in both reflections. The slight difference is 0006 reflection has relatively stronger contrast. This should be the misoriented lattice planes are more sensitive in 0006 reflection.

However, there are some certain regions in 0006 reflection are obviously lighter than 11-20 on the same position. This is because the 1/3<11-20> basal plane dislocations are out of contrast on the 0006 reflection. For screw dislocations and edge dislocations, when $\boldsymbol{g} \cdot \boldsymbol{b} = 0$, the dislocations are out of contrast in the reflection images. For mixed dislocations, when $\boldsymbol{g} \cdot \boldsymbol{b} \times \boldsymbol{l} = 0$, the dislocation are out of contrast in reflection images. Where the **g**, **b**, **l** are the diffraction plane normal vector, Burgers vector, and the dislocation line direction, respectively.

3.2 Ribbon sample analysis

3.2.1 Early Stage of Polycrystallization

EFG method was introduced in chapter 1, with the advantages of being capable of producing samples in different shapes by appropriate use of dies. In this study, the sample shape is ribbon in general. Detailed X-ray topography imaging of samples is carried out. The idea is to record reflection 11-20 (along growth direction) and the 1-100 topographs focusing on the area prior to initiation of polycrystallinity. Two reflections 11-20 and 1-100 are presented in Figure 3.5.

In these images, we found the blue ellipse regions have stronger contrast in both reflections. It is believed that these areas have high strains, which somehow change the orientation of lattice planes, causes the diffraction intensity change. The positions of high strains areas are coincident with our guess of initiation of polycrystallinity. Detailed images are provided in Figure 3.6.

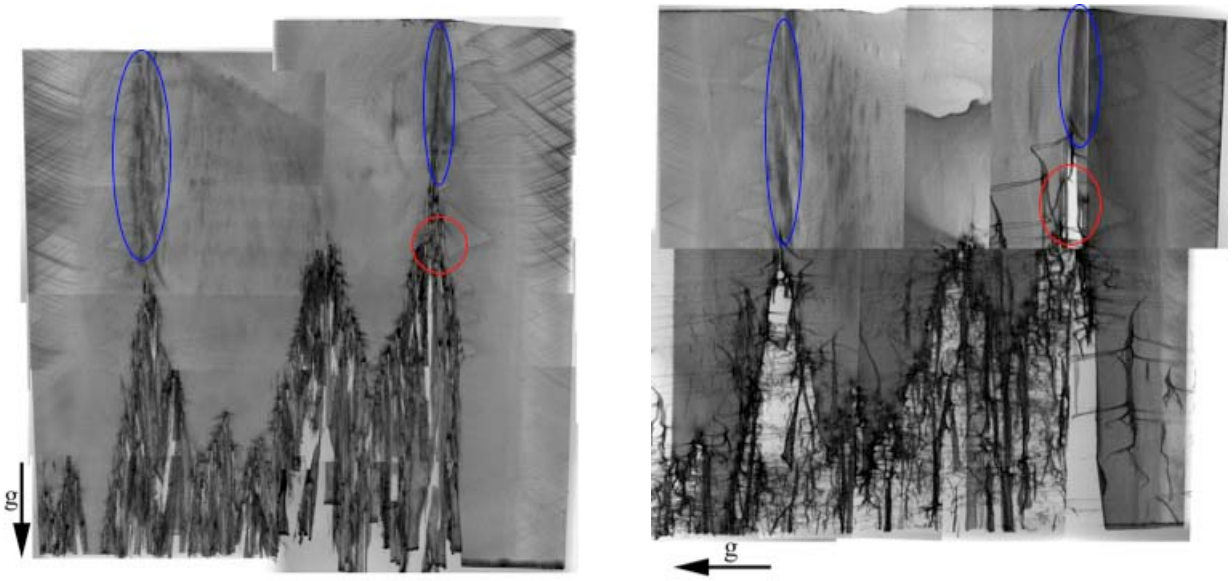

(a) g= 11-20 (b) g= 1-100

Figure 3.5 reflections 11-20 and 1-100 taken by Synchrotron White Beam X-ray topography on the same area, the surface of sample is (0001). From these two images, high strains, BPDs, and grain boundaries can be found.

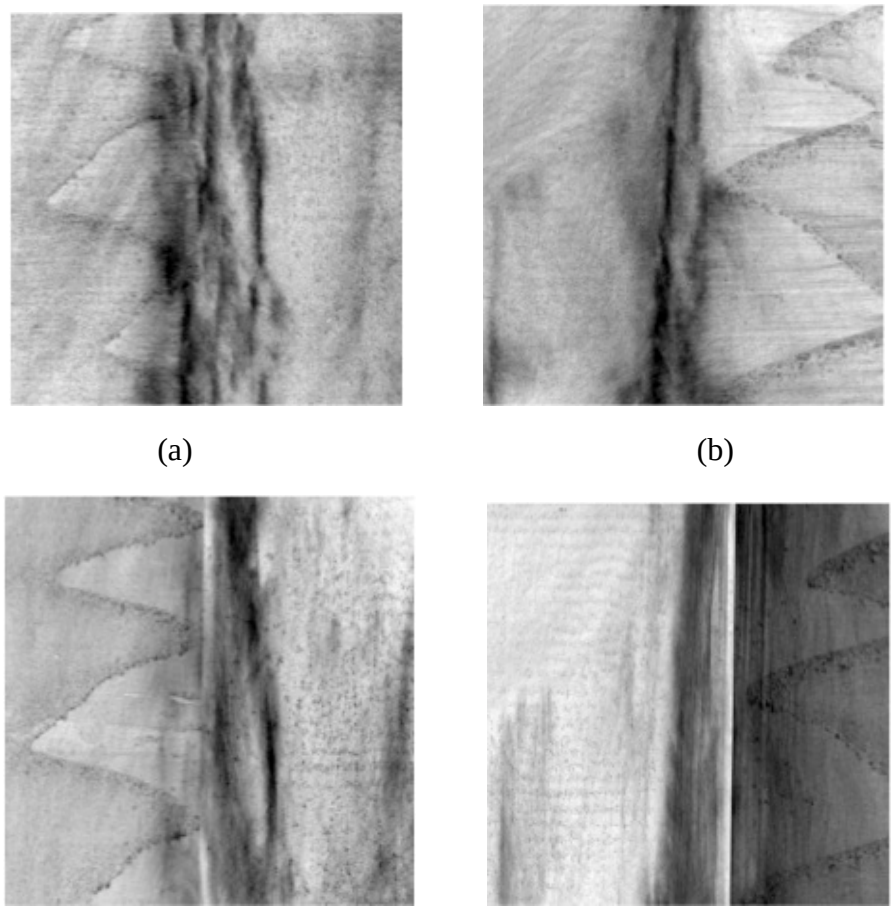

Figure 3.6 Detailed section images taken from Figure 3.5, (a) and (b) are around left and right blue ellipses regions of reflection 11-20, (c) and (d) are left and right blue ellipses regions of reflection 1-100.

Also, these regions have high density of BPDs, which actually is one of important reasons of the cause of high strains. BPD line deforms the atom array around it, which gives rise of strain. In this case, network of BPDs can be reasonable explain of high strains.

Furthermore, from these magnified images, features are much clearer. There are some wavy features on all four images. Actually, these are optically visible, and are some surface features. Probably, they are steps left by dislocation movement to surface. Or some growth vestiges caused by the fluctuations during growth.

3.2.2 Points of Polycrystallinity Nucleation

Tracking the dark contrast lines on Figure 3.5 all the way down, after the early stage of high strain and high density BPDs regions, we focus on the points of polycrystallinity nucleation. Magnified images are showed in Figure 3.7.

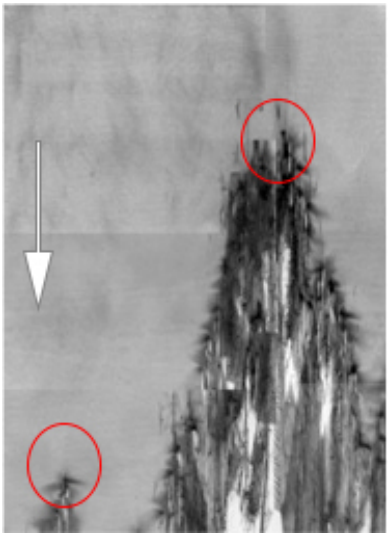

(a) g=11-20

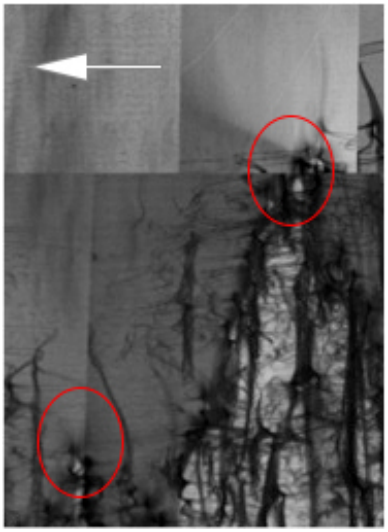

(b) g=1-100

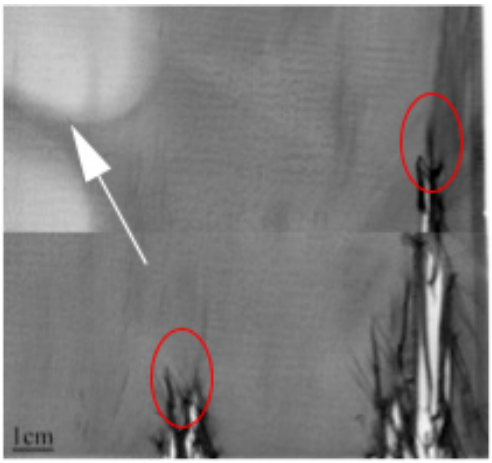

(c) g=01-10

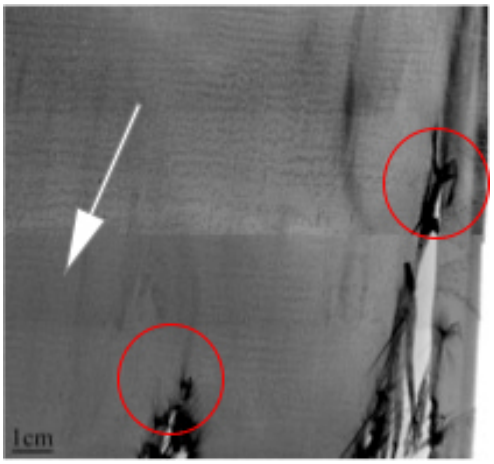

(d) g=10-10

Figure 3.7 Magnified images taken from Figure 3.5 for detail analysis. Those red ellipses are the nucleation points of grain boundaries.

From Figure 3.7, we can clearly see points of nucleation of grain boundaries, and the formation of polycrystallinity in sample. It appears to be a consequence of high density of BPDs aggregating, which finally forms tilt boundary. Imagine a crystal is bent about z-axis under external force, and dislocations are introduced to lower the energy associated with bending. Then dislocations move on their glide planes to rearrange as a vertical wall. With further bending, more dislocations are introduced, and the vertical wall forms to tilt boundary. Figure 3.8 illustrates the mechanism of tilt boundary formation.

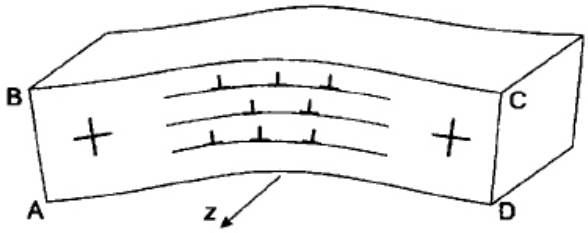

(a)

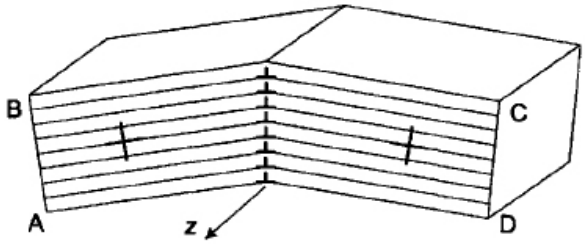

(b)

Figure 3.8 (a) dislocations are introduced; (b) dislocations rearrange to form tile boundary [19].

3.2.3 Reverse g-vector X-ray Topography

Although the tilt boundaries can be identified, but those dark and distorted peaks need to be studied in detail. Since the polycrystallinity images contain contributions from both strains and tilt boundaries, X-ray Topographs were recorded using a diffraction vector and again using by reversing the g vector. The geometry setting of reverse g-vector X-ray Topography is schematically shown in fig 3.9.

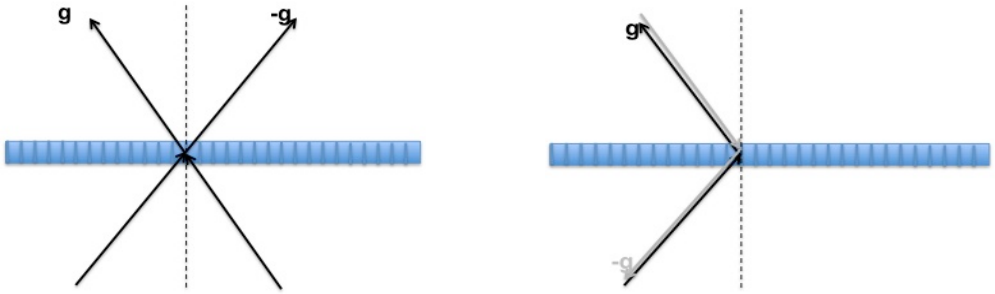

(a) (b)

Figure 3.9 Geometry of reverse g-vector setting of two different setting, (a) incident beam and diffraction beam at the same left or right side, surface of sample doesn't change for both g and –g reflection, (b) sample surface flipped to obtain g and –g reflection.

The reason using reverse g vector setting to distinguish between tilt boundaries and strains is based on the assumption that on reverse g vector reflections the strains and tilts will diffract differently. Two reflections -3300 and 3-300 are demonstrated in Figure 3.10.

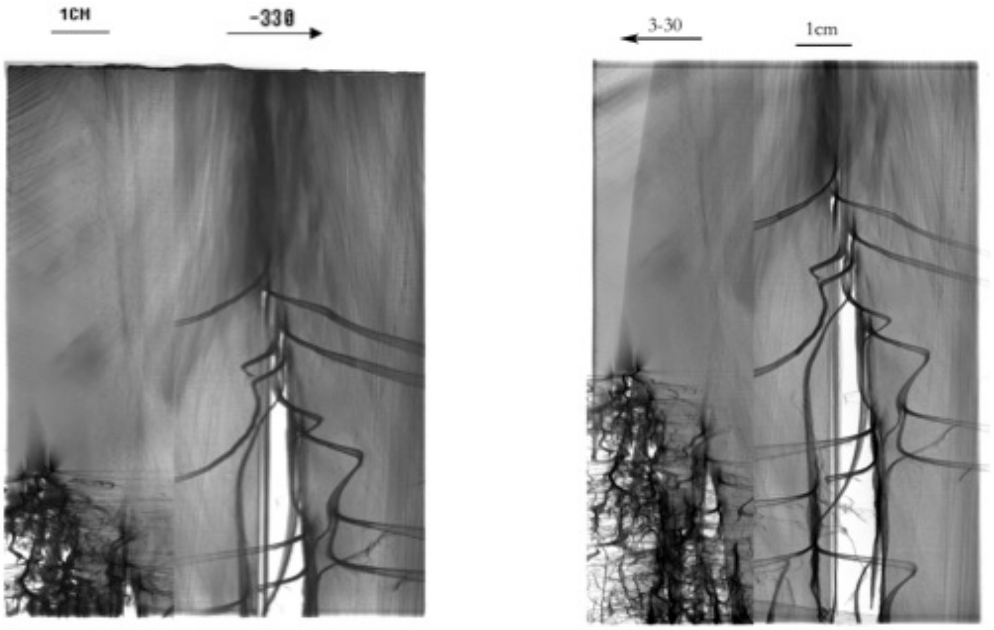

Figure 3.10 Reverse g reflections taken according to first setting in Figure 24, left one is reflection g= -3300, right one is reflection g= 3-300

And four more reflections taken according the second reverse g vector setting, following in Figure 3.11.

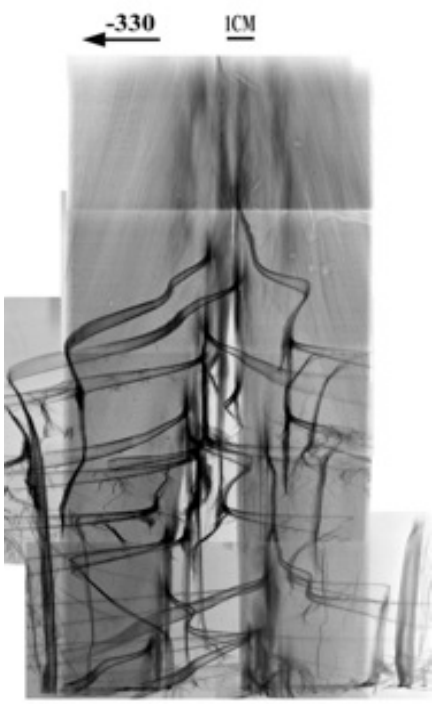

(a) g= -3300

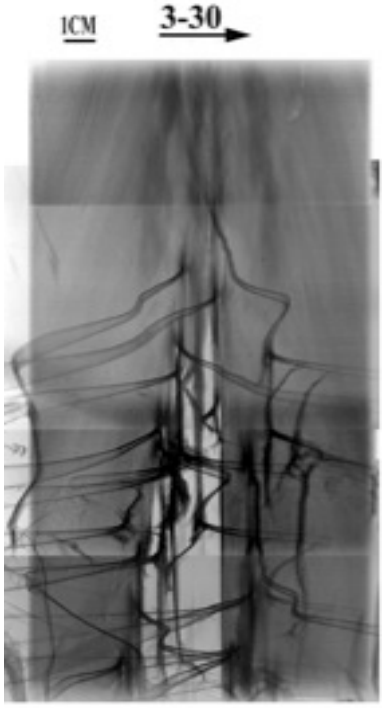

(b) g= 3-300

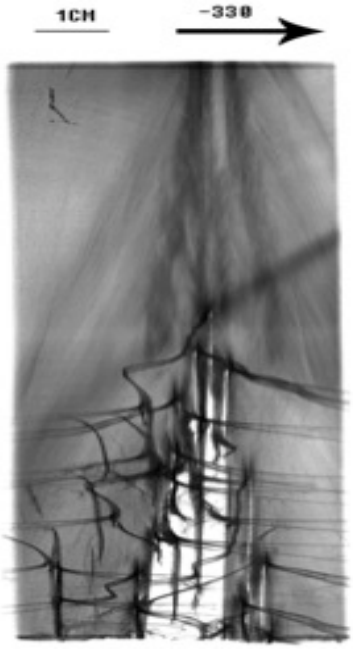

(c) g= -3300

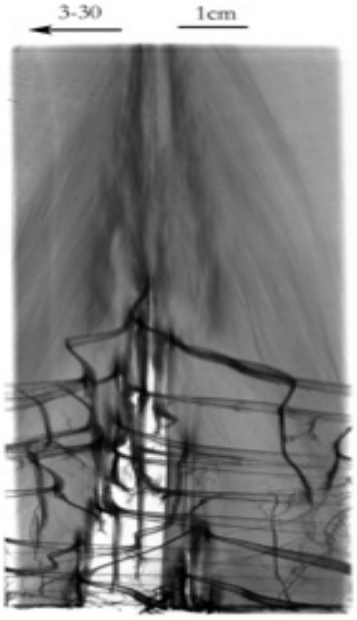

(d) g= 3-300

Figure 3.11 Figure 3.11 Reverse g reflections taken according to second setting.

From both Figure 3.10 and 3.11, we found there are no significant changes between reverse g vectors reflections. Only effect of reverse g-vector is to flip the direction of inhomogeneous strains i.e. tilt boundaries. Most of the distortion is due to rotation only. The reason we could not get expected images may be the g vector we chose is not sensitive in those lattice planes.

3.2.4 Determining the precise location of initiation of polycrystallinity

Transmission X-ray Topographs are projection topographs of the entire thickness of the sample and the depth information is not accessible. Therefore, to obtain depth of defect information, other X-ray Topography techniques are combined. In this study, we apply X-ray Section Topography to find out the exact initial point of polycrystallinity. The mechanism of X-ray Section Topography was introduced in section 2.1.3, and the procedure to determine the initial point is explained. A precision slit is used restrict beam height in our experiment to about 20 micron, o. A reference point was marked initially by using burn paper. Then, a series of X-ray Section Topograph were recorded by moving the sample up vertically by small steps. So, after several steps, a large area of sample is covered. At last, we put section steps together to have better idea about the polycrystallinity trend of the entire sample. Section steps are presented in Figure 3.12.

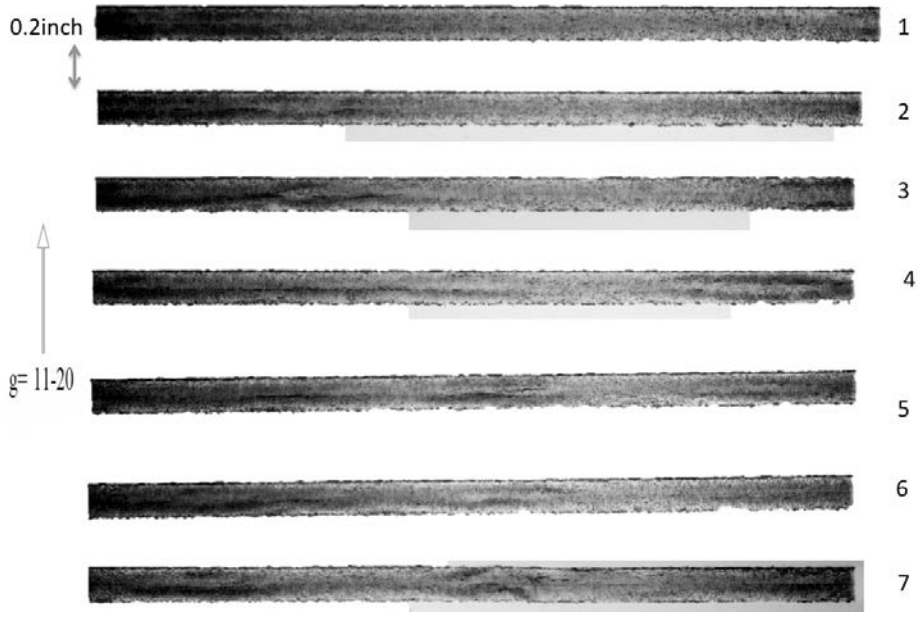

(a)

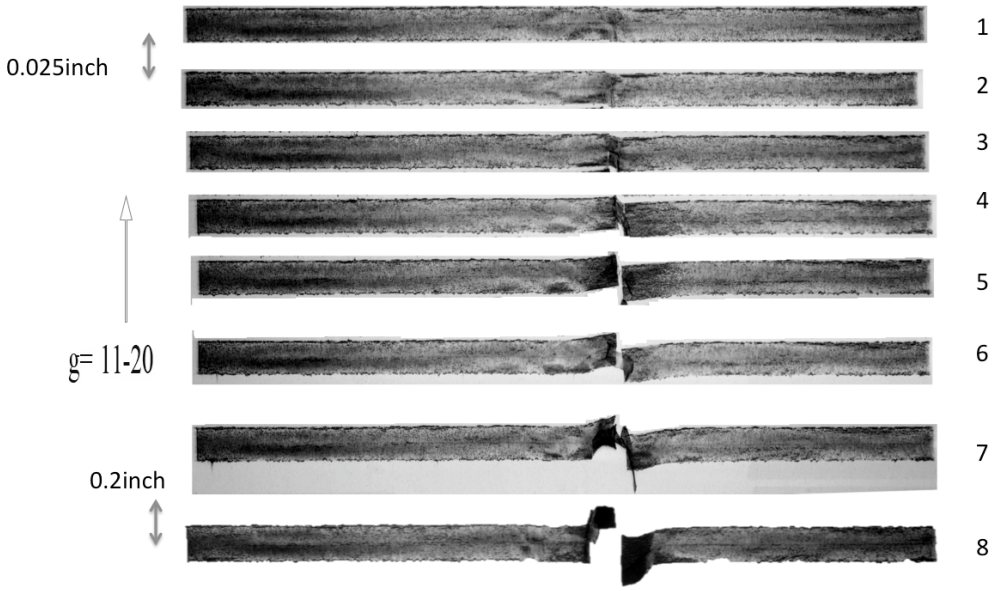

(b)

Figure 3.12 X-ray Section Topography (g = 11-20), (a) the distance between each step is 0.2 inch, (b) the distance between first 6 steps is 0.025 inch, around the point of initiation of polycrystallinity.

From Figure 3.12, we can clearly see the formation steps of grain boundary, which is the first sign of polycrystallinity. In Figure 3.12 (a), we can track the contrast changes from dark to light around the middle region of reflections. But there are no significant signs of grain boundary come up. Then, look at Figure 3.12 (b), the contrast around middle region starts significant change. Some very dark points come up on step 1 and 2. Further study on step 3, we found contrast missing, which the contrast becomes discontinuous. Looking further to following steps, the contrast interrupt becomes more obvious.

The reason we say the blank areas on those steps as contrast missing, due to orientation contrast caused by misorientation of planes around grain boundary. As introduced in section 2.1.1, diffraction occurs if it matches the Bragg's law. In this case, In this case, misorientation of planes changes the angles against the incident beam, which are no longer Bragg angles. But, since the white beam is used in this study, among so many different wavelengths, there must one match with the changed lattice plane in Bragg's Law. However, the diffracted locations are different, which results in separation or overlap with nearby grains. Figure 3.13 illustrates the schematic of diffraction due to lattice planes misorientation.

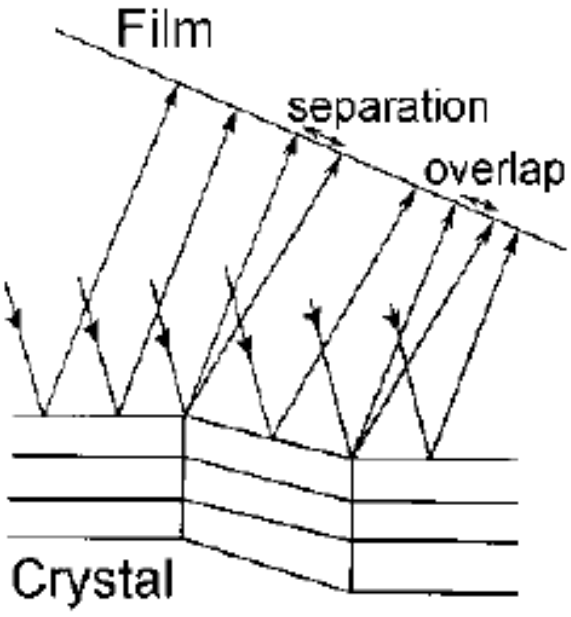

Figure 3.13 Schematic of diffraction due to lattice planes misorientation [20].

Based on the analysis of the section topograph images, we confirm that the initial point of crystallization is at step 3 of Figure 3.12 (b). After identifying the initial point, we can use the reference point to find the actual position on the sample.

3.2.5 Residue Stress field Mapping

To better understand the nature of stress and/or orientation variation in the samples, we do residual stress field mapping by applying X-ray Reticulography. The mechanism of X-ray Reticulography was introduced in section 2.1.4. Figure 3.14 shows the X-ray Reticulography images we get.

To map the stress field, we need quantitative results. Figure 3.15 shows how shear stress changes the lattice planes, and deformation of lattice planes changes the diffraction beam. In Figure 3.15 Strain is defined as the tangent of the angle α when a small element is sheared. Diffracting plane will automatically select the wavelength in the white beam, which satisfies the Bragger's law. Plane normal is tilted due to strain and it results in the shift (ΔS) of the diffracted spot, then shear strain can be measured by selecting appropriate diffraction and equation $\gamma_{xy} \sim \tan\alpha \cong \alpha = \Delta S/2L$.

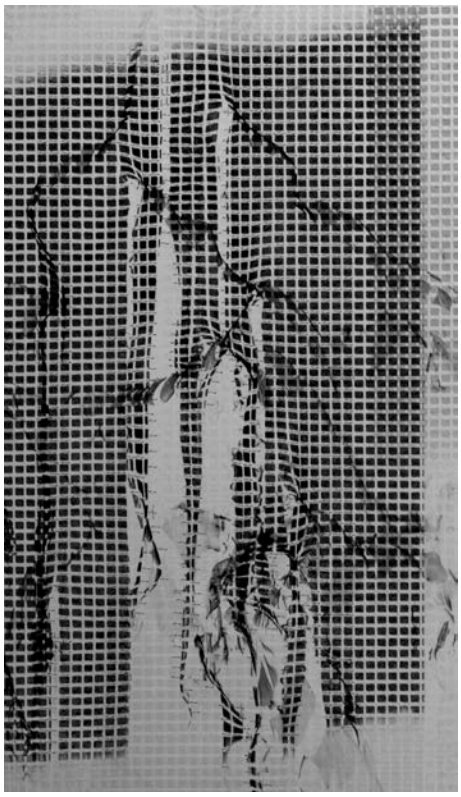

Figure 3.14 X-ray Reticulography image.

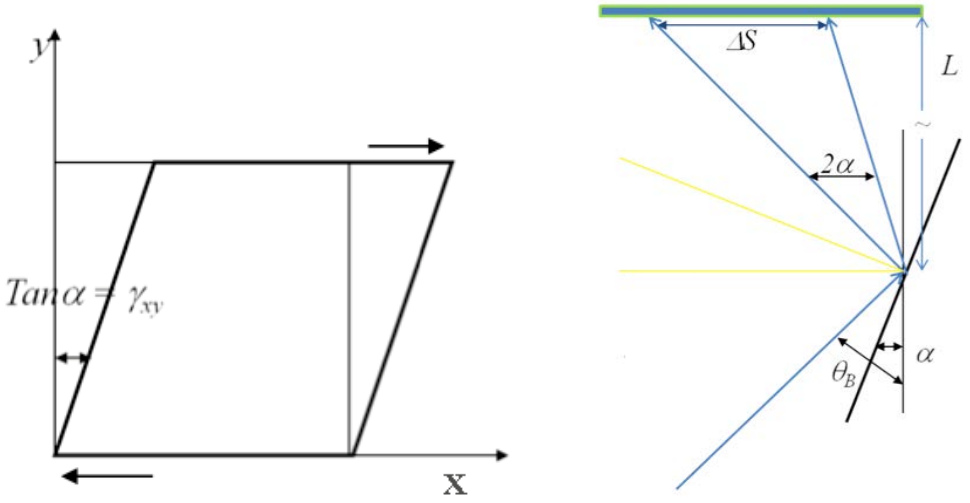

(a) (b)

Figure 3.15 Figure 3.15 (a) Schematic of simple shear of an area element in the xy plane; (b) Tilt (α) of lattice planes produces shift in diffracted beam (orientation contrast)

After get strains, then calculation of stress can be processed. In this study, the calculation is based on the formula

$$\tau = \gamma G \qquad \text{Equation 3}$$

Where τ is shear stress, γ is shear strain, and G is Shear Modulus, which is 145GPa in this calculation.

Finally, use different colors to present stress values on image to give more direct presentation. The mapping result we obtain is showed in Figure 3.16. The white color means zero stress, the blue area stress is 0-25 MPa, while green is 25-50MPa, yellow is 50-100MPa, red is 100-150MPa, and black is >150MPa.

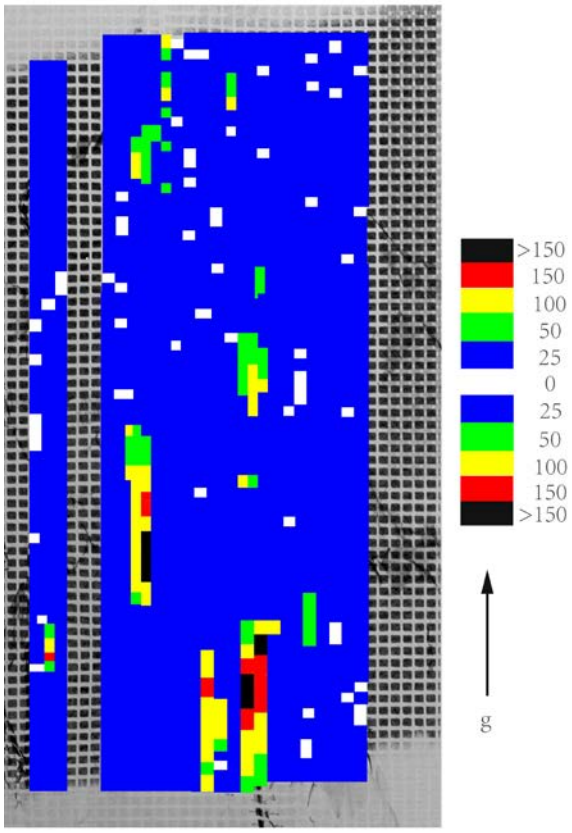

Figure 3.16 Residue stress field mapping

The mapping result shows the regions around the grain boundaries have bigger stress, which is coincident with our early study.

3.3 Chemical etching result

C-plane sapphire sample containing polycrystallinity region was selected for etching studies. Figure 3.17 presents the images taken by optical microscopy after etching. The etch pits are triangular in shaped and randomly dispersed. They are intersections of dislocation on the crystal

surface, which is c-plane in this case. The intersections are deformed by the dislocations, and chemically more reactive. So, their etching speed is higher than the rest of area, which revealed as etch pits.

It also shows a cluster of triangles lining up in the Figure 3.17, which is considered as the early stage of tilt boundary formation. As we discussed in section 2.3, many steps are left after dislocations move to surface. In figure 3.18, etch pits lining up parallel to those steps, rather than randomly dispersed, which is the evidence that those steps are left by complete moving of dislocations.

Also, in figure 3.19, another shape of etch pits are found, which are close to hexagons. This image is taken from another etched sample, which was etched for a longer period. And it turns out sample etching level is higher than the previous one. In another word, the size of etch pits can be bigger by increasing etching time. It can be clearly explained in Figure3.20.

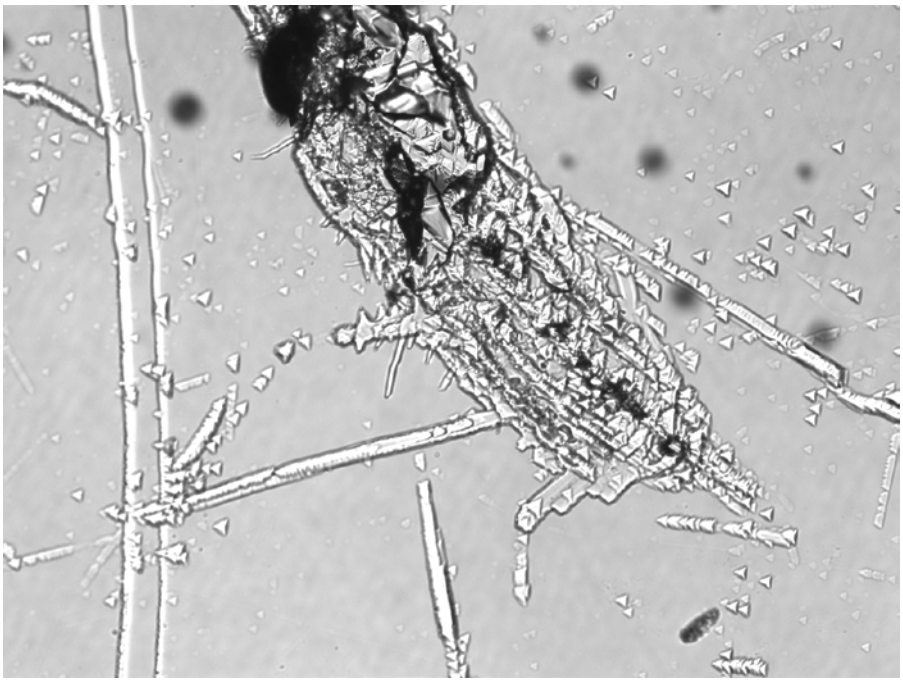

Figure 3.17 Etch pits found under microscopy.

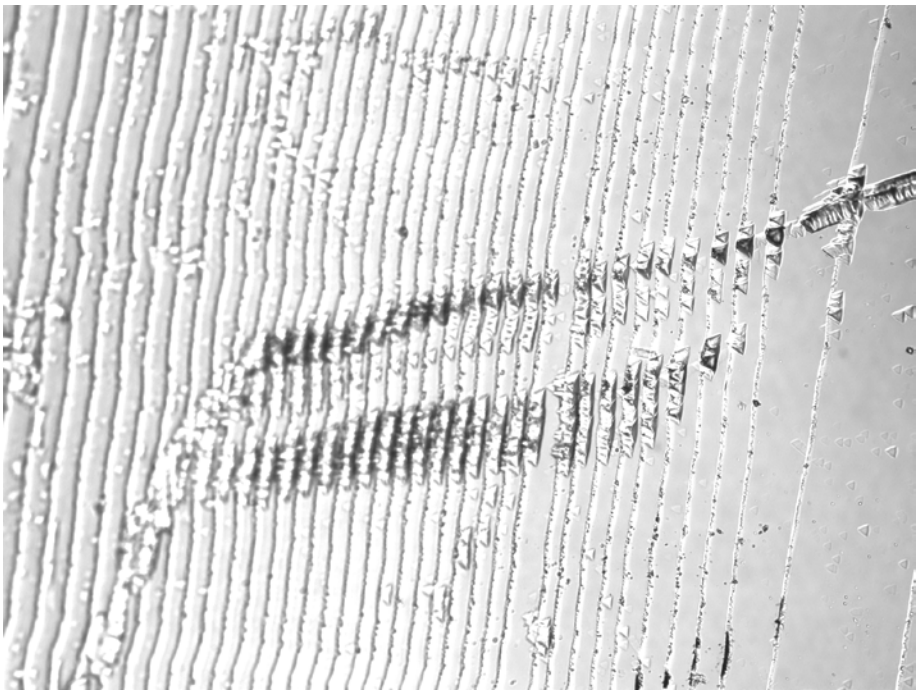

Figure 3.18 Etch pits lining up parallels to steps.

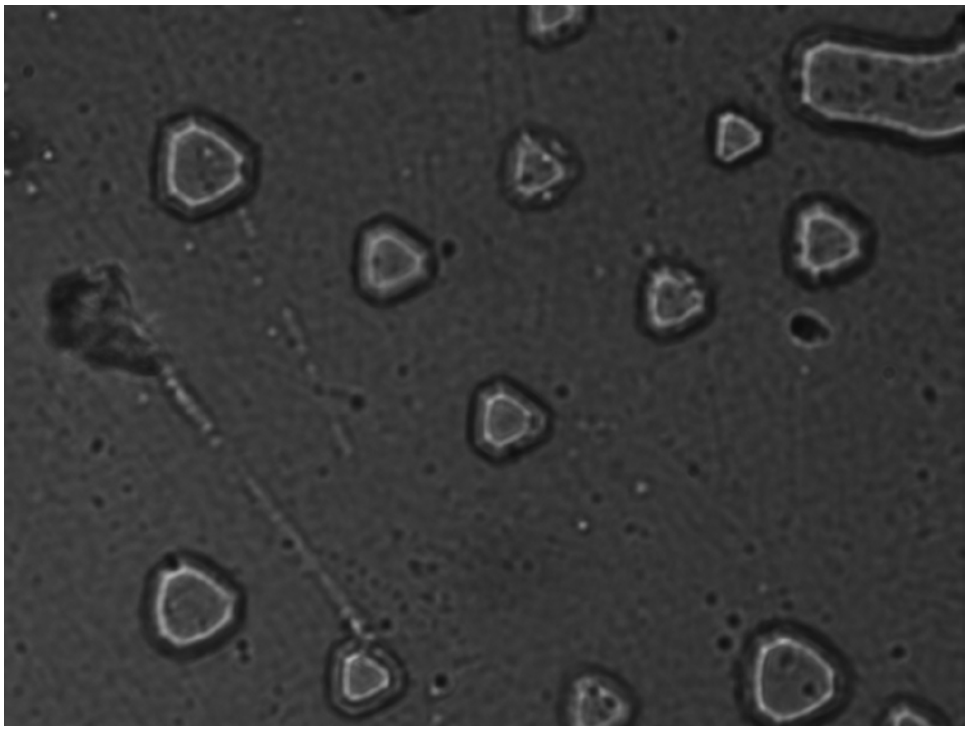

Figure 3.19 Etch pits in hexagon.

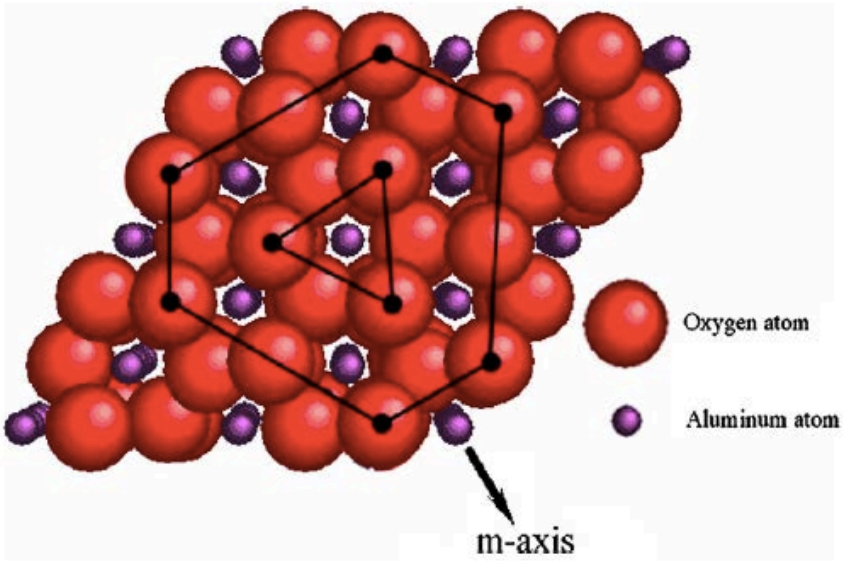

Figure 3.20 Atom arrangement of sapphire on (0001) plane [18].

From Figure 3.20, we can see, if the first middle aluminum atom removed, the etch pit appeared as triangle. With chemical etching processing, then three oxygen atoms removed on the second layer, which forms pseudo-hexagon etch pit as a result.

Conclusion

The thesis research focuses on defect analysis of EFG-grown sapphire single crystal ribbons by using Synchrotron White Beam X-ray Topography technique, Chemical Etching and as well as other techniques. The defects structures, properties and forming mechanisms are studied in detail.

Analysis and comparison of used seed and new seed crystals for EFG growth reveals the effect of growth on defect distribution within the seed. It is very important to have a high quality crystal seed, because defects can transfer or replicate to growing crystal. The detailed study on seeds reveals high strains and high density BPDs exist in regions of both two seed samples. Some surface scratches are observed as well. It is found that the used seed has fewer scratches than the new seed, which may be healed due to annealing effect.

As-grown c-plane sapphire ribbons were then studied using Synchrotron White Beam X-ray Topography. Scans of entire samples were recorded. And the topographs give the overall ideas about the quality of samples, by providing information of strains, dislocations and grain boundaries. Regions of polycrystallinity as revealed by darker and distorted contrast were isolated for more detailed studies.

Analysis of regions of dark contrast reveals networks of BPDs. These BPDs deform atom array around them, which result in high strains. These BPDs subsequently result in formation of grain boundaries, which are revealed by orientation contrast. The precise start point of polycrystallization was identified using X-ray topography in combination with X-ray Section Topography. Also, the residual stress fields were mapped by using X-ray Reticulography.

Chemical etching is applied to reveal dislocations on sapphire surface, which is c-plane in this study. The results from chemical etching complements and confirms results from X-ray Topography.

Reference

1. World of Crystals, http://www.mtberlin.com/frames_cryst/descriptions/sapphire.htm

2. Dobrovinskaya, R., Lytvynov, A., Pishchik, V., *Sapphire: Material, Manufacturing, Applications*, 2009, p. 55-56

3. Dobrovinskaya, R., Lytvynov, A., Pishchik, V., *Sapphire: Material, Manufacturing, Applications*, 2009, p. 56-57

4. Yougui Liao, *Practical Electron Microscopy and Database*, 2nd edition, 2007

5. F. A. KrÖger and H. J. Vink, *Relations between the Concentrations of Imperfections in Crystalline Solid*, Solid State Physics, Vol. 3 (1956), pp. 307-435

6. W. D. Kingery, Advances in Ceramics, Vol. 10, pp. 238-257

7. D.Hull and D.J. Bacon, *Introduction to dislocations*, 4th Ed., p. 11

8. B. D. Cullity, *elements of X-ray diffration,* 2nd Ed., pp. 59-62

9. M. J. BUERGER, American Mineralogist, Volume 30, pp. 469-482, 1945

10. Huili Tang, Hongjun Li, Jun Xu, February 20, 2013, *Growth and Development of Sapphire Crystal for LED Applications,* Advanced Topics on Crystal Growth, P. 317

11. Chun-Hung Chena, Jyh-Chen Chena, Chung-Wei Lub, Che-Ming Liuc, *Numerical simulation of heat and fluid flows for sapphire single crystal growth by the Kyropoulos method*, Journal of Crystal GrowthVolume 318, Issue 1, 1 March 2011, Pages 162 – 167, The 16th International Conference on Crystal Growth (ICCG16)/The 14th International Conference on Vapor Growth and Epitaxy (ICVGE14)

12. Mark S. Frank J. Brunib, *Modern trends in crystal growth and new applications of sapphire*, Volume 360, 1 December 2012, Pages 134 – 145, 5th International Workshop on Crystal Growth Technology

13. F. Schmid, D. Viechnicki, *Growth of sapphire disks from the melt by a gradient furnace technique,* Journal of American Ceramics Society, 53 (1970), p. 528

14. Mark S. Frank J. Brunib, *Modern trends in crystal growth and new applications of sapphire*, Volume 360, 1 December 2012, Pages 134 – 145, 5th International Workshop on Crystal Growth Technology

15. Raghothamachar, B., et al., *Defect analysis in crystals using Sychrotron X-ray Topography.Microsc*, Res Tech, 2006. 69(5): p.343-58.

16. B. K. Tanner, M. A., D. phil., *X-ray Diffraction Topography,* 1st Ed, 1976, pp. 68-69

17. Vish Sarkar, *Defect Characterization and Stress Analysis by White Beam Synchrotron X-ray*

Topography in Single Crystal Semiconducting Materials, p. 26

18. Vish Sarkar, *Defect characterization and stress analysis by white beam synchrotron X-ray topography in single crystal semiconducting materials*, p. 16

19. D.Hull and D.J. Bacon, *Introduction to dislocations*, 4th Ed., p. 160

20. Raghothamachar, *Synchrotron White Beam X-ray Characterization of Growth Defects in Bulk Compound Semiconductors,* p. 43

21. Che-Ming Liu, Jyh-Chen Chen, Yi-Cheng Huang, Hung-Lin Hsieh, *The morphology of etch pits on a sapphire surface*, Journal of Physics and Chemistry of Solids 69 (2008) 572–57